Dynamics on Networks and Lattices

Vidit Agrawal

A dissertation submitted for the partial fulfilment
of BS-MS dual degree in Science

Indian Institute of Science Education and Research Mohali
April 2014

Certificate of Examination

This is to certify that the dissertation titled **Dynamics on Networks and Lattices** submitted by **Vidit Agrawal** (Reg. No. MS09134) for the partial fulfillment of BS-MS dual degree programme of the Institute, has been examined by the thesis committee duly appointed by the Institute. The committee finds the work done by the candidate satisfactory and recommends that the report be accepted.

Dr. Abhishek Chaudhuri Dr. Kamal P. Singh Dr. Sudeshna Sinha (Supervisor)

Dated: April 24, 2014

Declaration

The work presented in this dissertation has been carried out by me under the guidance of Prof. Sudeshna Sinha at the Indian Institute of Science Education and Research Mohali.

This work has not been submitted in part or in full for a degree, a diploma, or a fellowship to any other university or institute. Whenever contributions of others are involved, every effort is made to indicate this clearly, with due acknowledgement of collaborative research and discussions. This thesis is a bonafide record of original work done by me and all sources listed within have been detailed in the bibliography.

Vidit Agrawal
(Candidate)

Dated: April 24, 2014

In my capacity as the supervisor of the candidates project work, I certify that the above statements by the candidate are true to the best of my knowledge.

Prof. Sudeshna Sinha
(Supervisor)

Acknowledgment

I would like to thank Prof. Sudeshna Sinha for her guidance and support in the successful completion of my final year thesis project.

Vidit Agrawal

List of Figures

Notation

Chapter-1

ϵ	Coupling Parameter
p_s	Probability of random links
p_t	Probability of link change
η	site of 1^{st} neighbour (randomly chosen with probability p_s and regularly chosen with (1 - p_s))
ξ	site of 2^{nd} neighbour (randomly chosen with probability p_s and regularly chosen with (1 - p_s))
Z(n)	Synchronization error function
T_{sync}	Time to reach synchronization
$L_{intermittant}$	Time duration of intermittant behavior

Chapter-2

τ_0	Total period of disease cycle
τ_I	Period for which individual is infected
τ_R	Period for which individual is refractory/immune
S_0	Initial fraction of Susceptible individuals in the population
R_0	Initial fraction of Refractory individuals in the population
I_t	Fraction of Infected individuals in the population at time 't'
η	Initial fraction of refractory population having randomly different phases
χ	Range from which initial phases of refractory individuals is taken

Abstract

Chapter-1 Connection topology is the key to controlling the spatio-temporal dynamics of coupled maps, and varying the fraction of random links can tune the system from spatio-temporal chaos to synchronized stable fixed points. Here we consider a network of chaotic maps, where the sites connect to nearest neighbours with probability $(1-p_s)$, and to random non-local sites with probability p_s. Further we consider that the underlying links in the system can switch with probability p_t, keeping the average fraction of random links the same. This implies that when p_t is unity, the links in the network change at each iteration, with the new links being random with probability p. We study two kinds of variation of the links. We consider the scenario where the links change independently at the local level, namely, the coupling connections of every node is switched with probability p_t. Our central result is that the probabilistic switching of links, at the local or global level, yields a sharply increasing range of synchronized fixed point, as one goes from a completely static network to completely dynamic one. Further, for small p_t, we observe that different realizations of the connectivity matrix, with the same fraction of random links, synchronizes at different values of coupling strength, and so there is a spread in the values of the critical coupling strength necessary for synchronization. However, as we go towards the completely dynamic limit ($p_t = 1$) there is rapid convergence to a specific critical coupling strength, indicating that dynamic rewiring acts like a self-averaging mechanism, as the network evolves under many different connection matrices drawn from an ensemble of matrices with the same p, over time. The enhanced spatio-temporal regularity obtained under dynamic links is also verified through linear stability analysis about the synchronization manifold. Lastly, for low probabilities of link change, we find that the system shows intermittency, and as the links switch more frequently, this intermittency gives way to perfect synchronization.

Chapter-2 We investigate the emergent infection spreading patterns in a population on 2-Dimensional lattice based on a cellular automata model of the SIRS disease cycle. We observed that in a population consisting of randomly distributed refractory and susceptible individuals, an infection seed can lead to persistent infection in the population. Further, our results suggest that the size of the infected sub-population depends on the dynamical characteristics of the disease cycle, and on the heterogeneity of the population in which the disease spreads.

Contents

Chapter 1

Regularizing influence of Dynamical Links

1.1 Introduction

Networks of coupled dynamical systems capture the essential spatiotemporal features of large interactive systems with complex dynamics at the local scale [13]. Most studies so far have focussed on static networks. However, in many realistic scenarios the links between the constituent sub-systems are likely to change over time. In fact a wide range of extended systems of biological, technological and physical significance are better described by a dynamically changing web of connections. Motivated by this, we will study the spatiotemporal dynamics of networks of coupled systems where the links change with a certain prescribed probability.

1.2 Model

We consider a one dimensional ring of coupled strongly chaotic logistic maps. The sites are denoted by $i = 1, 2, 3, ...N$ where N denotes the linear size of the lattice. The evolution of this lattice, in discrete time n is given by

$$x_{n+1}(i) = (1 - \epsilon) f[x_n(i)] + \frac{\epsilon}{2}\{x_n(\xi) + x_n(\eta)\} \tag{1.1}$$

where,

$$f(x) = 4x(1 - x) \tag{1.2}$$

and ϵ is the coupling strength.We also define a parameter p_s which represents the probability of links being random. Here, $\xi = i + 1$ with probability $1 - p_s$ and is a randomly chosen integer ξ $(1 \leq \xi \leq N)$ with probability p_s. Similarly, $\eta = i - 1$ with probability $1 - p_s$

and is a randomly site with probability p_s. The $p_s = 0$ case corresponds to regular nearest neighbour coupling and $p_s = 1$ corresponds to completely random connections.

Now we consider a situation wher the connections in the network can vary in time. If the switching of links occurs at every dynamical time step, then it is a completely dynamic networks, aqnd if ξ and η do not change in time then it is a completely static network. Our focus here is to study the transition between these two limits. We do this through a parameter p_t which gives the probability with which a link in the network can change. If $p_t = 0$ then we have the case of quenched links (ξ and η fixed in time) and if $p_t = 1$ then all links switch at every time step.

So the link switching criterion is local, and the links of every node(site), at every instant of time, can change independently with probability p_t. It is evident then, that if a node swtiches links at a certain point in time, the other nodes may or may not switch their connections. The frequency of changing connections, on an average, is determined by the probability p_t. This is in contrast with the network changing all the links globally with a certain probability, i.e. the scenario where the entire connectivity matrix of the network changes at certain points in time.

In this work, we investigate the asymtotic dynamics of this network, evolving from random initial conditions. Specifically, we examine the spatiotemporal implications of varying the coupling strength ϵ, and the link switching probabilty p_t.

1.3 Analysis

Through extensive numerical simulations of this dynamical network we obtain bifurcation diagrams with respect to couplinbg strength ϵ. From these bifurcation diagrams we find the critical coupling strength ϵ_c such that one obtains spatio-temporal syncronization, namely a spatio-temporal fixed point, for $\epsilon \geq \epsilon_c$

1. $p_t = 1.0, p_s = 1.0$. This is the regime where one has a completely random network with the links switching at every iteration. Fig. 1.3-[top-left] shows that the critical coupling strength $\epsilon_c \approx 0.54$.

2. $p_t = 1.0, p_s = 0.65$. Here links are switched at every time step. However, the probability of these links being spatially random is reduced. Fig. 1.3-[top-right] shows that this decrease in randomness in spatial connections reduces the range of spatiotemporal syncronization, with the critical coupling strength now being $\epsilon_c \approx 0.62$.

3. The case of $p_t = 0.5, p_s = 0.65$ is displayed in Fig. 1.3-[bottom-left] and that for $p_t = 0.1, p_s = 0.65$ in Fig. 1.3-[bottom-right]. With decreasing p_t, at fixed p_s, the critical coupling strength ϵ_c increases from ≈ 0.66 for $p_t = 0.5$ to ≈ 0.91 for $p_t = 0.1$. Namely as the probability of changing links decreases, the range for the spatio-temporal fixed

point decreases. So a more dynamic web of links is more favourable for inducing spatiotemporal regularity in coupled chaotic systems.

Now, we consider low probability of link change, namely a network near the static limit, with p_t close to zero. The analysis in this regime is complicated by the fact that one obtains a range of critical coupling strengths, with ϵ_c being strongly dependent on the initial configuration of links. A deeper understanding is gained by studying the distribution of ϵ_c, at fixed p_t and p_s, for different initial conditions, as displayed for representative cases in Fig. 1.2.

It is clear from Fig. 1.2 that for the case of $p_t = 0.0$, i.e. a static network with quenched links, there is a spread of critical coupling strengths ϵ_c, with the range being approximately $[0.73 : 0.97]$, and the most probable value being ~ 0.85. As p_t increases, for instance when $p_t = 0.01$, we observe that the spread of critical coupling strength ϵ_c narrows considerably, and the most probable value alo shifts to a smaller value. Lastly, for the limiting case of $p_t = 1.0$, it is clear that the critical coupling strength ϵ_c rapidly converges to a single value. This is a reflection of the "self-averaging" arising from dynamically changing links, as p_t becomes larger.

Now we analyze the variation of the average critical coupling strength $\langle \epsilon_c \rangle$ with respect to the probability of link change p_t. Figs. 1.3 display the average critical coupling strength (in red), the maximum value of critical coupling strength ϵ_{cmax} observed (in green) and the mimimum value of critical coupling strength ϵ_{cmin} observed (in blue). From the plots it is evident that $\langle \epsilon_c \rangle$ diplays a clear trend under increasing p_t, even at low p_t when the ϵ_{cmin} and ϵ_{cmax} values are rather far apart.

1.3.1 Interplay of p_s and p_t on spatio-temporal regularity

The next part of our analysis is to uncover the effect of p_s on the dependence of the critical coupling strength $\langle \epsilon_c \rangle$ on p_t. In order to do this, we examine the $\langle \epsilon_c \rangle$ vs p_t curves for different values of p_s, and attempt to fit a suitable functional form to capture the trend.

We explored a power-law fit, given by:

$$\langle \epsilon_c \rangle = \frac{1}{(p_t)^a} + b \tag{1.3}$$

with a and b being the fitting paramters.

For the best possible curve fit analysis, we took the datapoints in the range $p_t = [0.25 - 0.75]$. Fig. 1.4 shows the data alongside the fitted curve.

The values of the fitting paramters a and b are tabulated below:

p_s	a	b
0.5	0.0656857	-0.328514
0.65	0.0724886	-0.384942
0.7	0.07449	-0.400539
0.8	0.0801529	-0.428067
0.9	0.0847064	-0.446896

Dependence of parameters a and b on p_s:

Fig. 1.5 shows the variation of fitting parameter a on p_s.

Fig. 1.5 shows the variation of fitting parameter b on p_s.

1.3.2 Synchronization

We now study the degree of syncronization in the system quantitatively through the synchronization error function defined as

$$Z(n) = \frac{1}{N}\sum_{i=1}^{N}[x_n(i) - x^*]^2 \tag{1.4}$$

averaged over time n and calculated after transient time. Here x^* is the fixed point for the logistic map equal to 0.75.

In the results displayed here, the synchronization error is averaged over 10000 time steps, after a transient time of 100 steps for 100 different initial conditions. The value of p_s is 0.65.

Fig. 1.7-[top] shows the variation of the averaged synchronization error $\langle Z \rangle$ (in red), the maximum synchronization error Z_{max} (in green), the minimum synchronization error Z_{min} (in blue) as a function of coupling strength ϵ, for $p_t = 0$ (i.e. a static network). At low coupling strengths ($\epsilon \in [0.0 - 0.1]$), and at very high coupling strengths ($\epsilon \geq 0.95$), $\langle Z \rangle$, Z_{min} and Z_{max} are equal, i.e. different initial conditions yield the same spatio-temporal dynamics. The range of coupling in-between these is of interest as a spread is observed here between Z_{max} and Z_{min}, implying that different initial conditions lead to different degrees of synchronization. However, the averaged synchronization error $\langle Z \rangle$ shows a clear trend, as it decreases with increasing ϵ, finally becoming zero at $\epsilon_c \approx 0.85$. That is, for $\epsilon \geq \epsilon_c$ we obtain complete syncronization. Another interesting observation is a dip at around $\epsilon = 0.2$, signifying enhanced synchronization around that coupling strength. This is due to the existence of stable 2-cycle over a small range of coupling strengths.

Fig. 1.7-[middle] shows the case of $p_t = 0.01$. Now the seperation in Z_{min} and Z_{max} is negligible for entire coupling range ($\epsilon \in [0.0 : 1.0]$), signifying that almost all initial conditions evolve to same spatio-temporal state, i.e. there exists a global attractor for the dynamics. The dip in $\langle Z \rangle$ is still discernable at around $\epsilon = 0.2$. The bifurcation diagram around this coupling strength is shown in Fig. 1.8.

Fig. 1.7-[bottom] shows the results for $p_t = 0.5$. The dip around $\epsilon = 0.2$ is gone and there is a smooth trend for $\langle Z \rangle$. This implies that the 2-cycle at weak coupling is destroyed when the links change too frequently. However at strong coupling the dynamic links stabilize a larger range for the spatiotemporal fixed point.

We have also studied the variation of Z with respect to p_t. Fig. 1.9 shows the variation of the averaged synchronization error $\langle Z \rangle$ (in red), the maximum synchronization error Z_{max} (in green), the minimum synchronization error Z_{min} (in blue) as a function of p_t, for coupling strength $\epsilon = 0.65$. It is evident that $\langle Z \rangle$ decreases as p_t increases upto a critical point $p_t \approx 0.54$, and there onwards is zero till $p_t = 1.0$. This implies that if the probability of changing links is higher than ~ 0.54, one obtains complete synchronization.

A noteworthy trend here is that the separation of Z_{min} and Z_{max} rapidly decreases as p_t increases.

Fig. 1.10 shows the variation of $\langle Z \rangle$ with changing p_t, for $\epsilon = 0.7$. In this case, the critical point after which complete synchronization is observed is around 0.28. Hence it is evident that at higher coupling strengths larger range of p_t exhibits complete synchronization.

1.4 Average time to reach Synchronization

We define an order parameter T_{sync}, which represents the time after which the network is completely syncronized. We then study its variation with respect to p_t and ϵ at different values of p_s. Specifically we calculate the average $\langle T_{sync} \rangle$, the maximum time $T_{syncmax}$ and minimum time $T_{syncmin}$.

Figs. 1.11 show the case of $p_t = 0.01$ and $p_t = 0.1$. The separation of the minimum and maximum values of T_{sync} is large for low ϵ which then decreases consderably at higher coupling strengths. Further for large p_t, i.e. when the links change frequently, the spread in synchronization time narrows considerably. This is a reflection of the self-averaging effect of dynamic links.

We further, explored the trend of $\langle T_{sync} \rangle$ under variation of p_s, p_t and system size N. We show representative cases in Figs. 1.12-1.14. It i clear that for smaller system, i.e. low N, the sudden drop in the time needed to reach synchronization begins at lower coupling strengths ϵ.

We have also investigated the dependence of the time needed to reach synchronization $\langle T_{sync} \rangle$ vs. p_t. Representative results are displayed in Figs. 1.15-1.17.

1.4.1 Intermittent approach to synchronization

The system here mainly exhibits two kinds of dynamics after transience, either it syncronizes to the fixed point completely or it stays chaotic. But here another regime is observed, where the system displays synchronized periods with bursts of unsyncronized behaviour. This is

illustrated by the time-series of a representative case shown in Fig. 1.18. As it can be seen, the system shows almost complete spatiotemporal syncronization around $t_1 = 2500$ for the first time, but subsequently loses it, syncronizing again around $t_2 = 4600$, after which it remains synchronized upto the limits of our simulation time.

We define a parameter Ł$_{intermittant}$ which reflects for the time duration of such intermittent behaviour. This is the time between the the first event of near complete spatiotemporal syncronization and the last unsynchronized burst observed. Specifically, without loss of generality, we consider a system synchronized if the synchronization error $Z < 0.00001$.

We find the average of this parameter over 100 diifferent initial, and we follow the system up to 5000 iterations. In particular, we study the dependence of the intermittent period on the coupling strength.

Figs. **??** show that there is no intermmitency, i.e. Ł$_{intermittant} = 0$, for the completely chaotic region at low coupling strengths, and the completely syncronized region at high coupling strengths. However, for a range of coupling around the critical coupling strength, the average length of the intermittent period increases and then decreases, reaching a maximum around ϵ_c. It is further evident that as the probability of changing links increases, the range of coupling strengths over which this intermittent approach to synchronization is observed, decreases.

Fig. 1.20 shows the dependence of the intermittent period on the probaility p_t of link change, and a similar qualitative picture is seen here as well.

1.5 Generality of Results

In order to gauge the generality of our results, we also analysed a network of Exponential Maps (also known as the Ricker Map). These are given by the dynamical equation:

$$f(x) = x\ e^{r(1-x)} \tag{1.5}$$

We take parameter r to be 2.6, where the map is strongly chaotic.

Representative results are shown in Fig. 1.21. Clearly, spatiotemporal synchronization is obtained at coupling strengths $\epsilon > \epsilon_c$, where $\epsilon_c = 0.48$ for $p_t = 1$.

Now, for 100 different initial conditions, the variation of $\langle\epsilon_c\rangle$, ϵ_{cmax} and ϵ_{cmin} with respect to p_t was calculated, and the results are displayed in Fig. 1.22. It is evident that the qualitative picture is same as in a network of chaotic logistic maps. Namely, we again observe a wider separation between ϵ_{cmax} and ϵ_{cmin} at very low p_t (.e. close to the static limit), and this shrinks rapidly as p_t increases. As before, we also find a smooth decreasing trend for $\langle\epsilon_c\rangle$ with increasing p_t. So it is clear that more frequent link changes enhances the range of spatiotemporal synchronization, with the critical coupling strength necessary

to obtain the spatiotemporal fixed point being lower in networks with faster variation in connectivity.

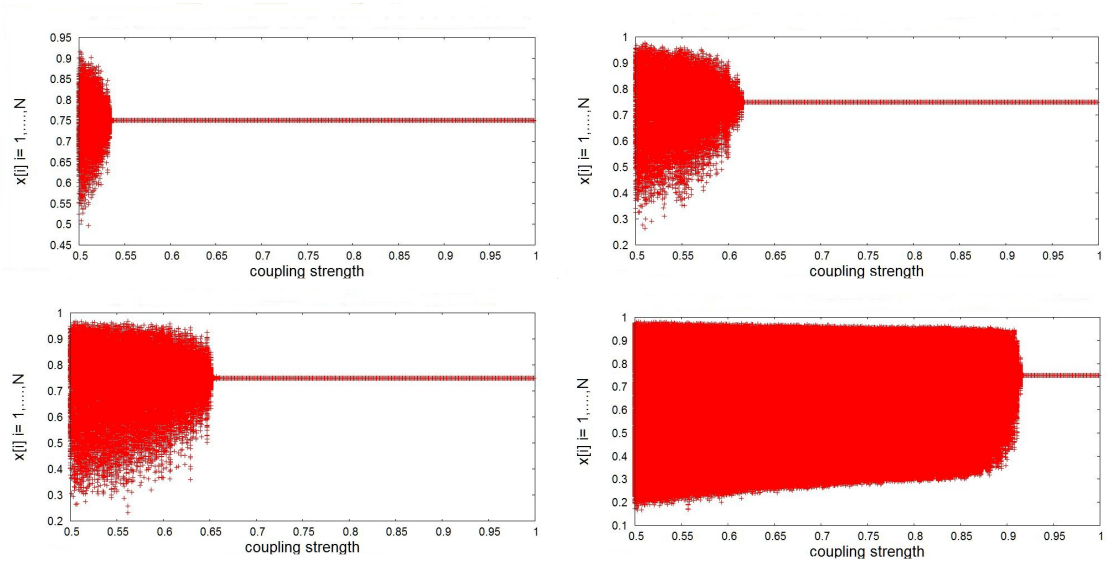

Figure 1.1: State of the system $x_n(i)$, $i-1,\ldots N$, for a network of size $N = 50$, with respect to coupling strength ϵ. The plot shows 5 superimposed iterates after 2000 transient steps, for 10 random initial conditions. $p_t = 1.0$ and $p_s = 1.0$ (top left); $p_t = 1.0$ and $p_s = 0.65$ (top right); $p_t = 0.5$ and $p_s = 0.65$ (bottom left); $p_t = 0.1$ and $p_s = 0.65$ (bottom right).

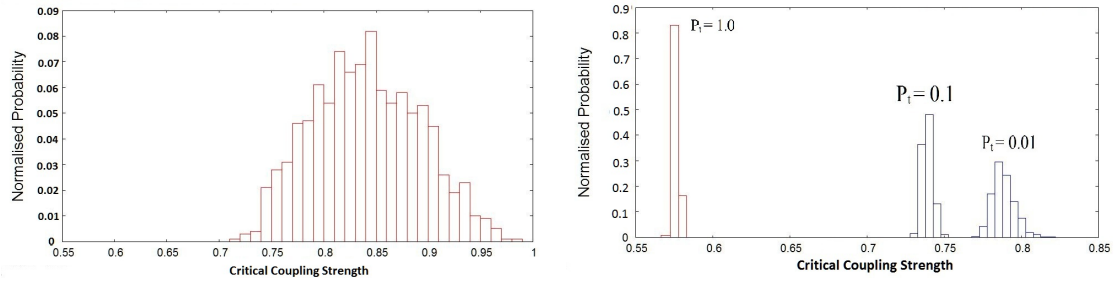

Figure 1.2: Distribution of critical coupling strengths ϵ_c obtained for a network of size $N = 50$ with $p_s = 0.65$ for 1000 different initial conditions. Here $p_t = 0.0$ (left); $p_t = 0.01, 0.1, 1.0$ (right).

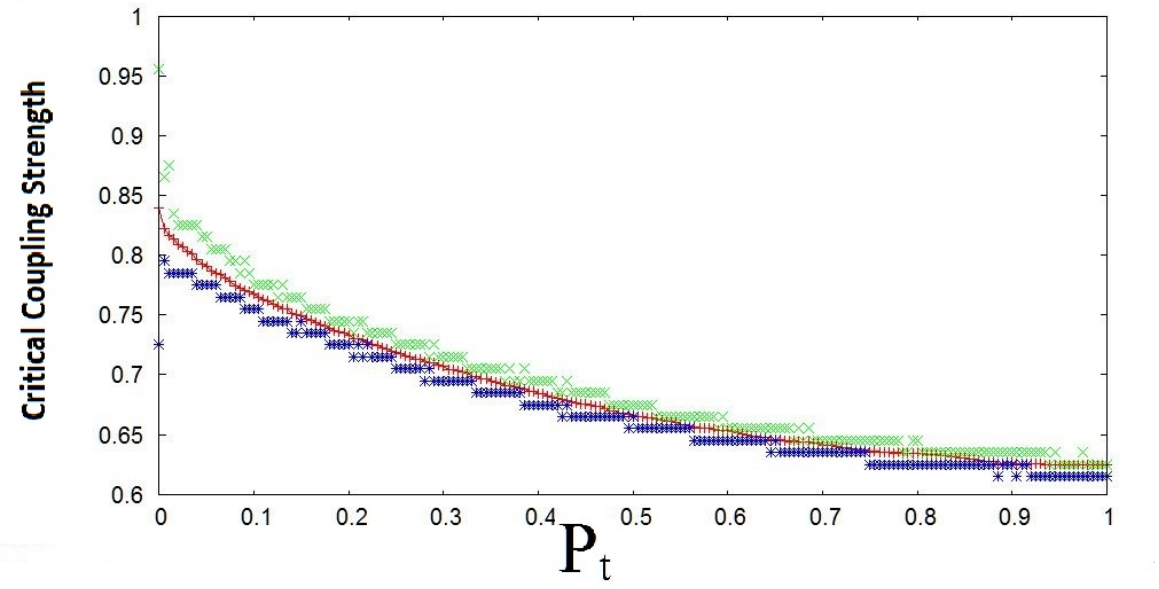

Figure 1.3: Averaged critical coupling strength $\langle \epsilon_c \rangle$ with respect to the probability of link change p_t, in a network of size $N = 50$, with $p_s = 0.65$.

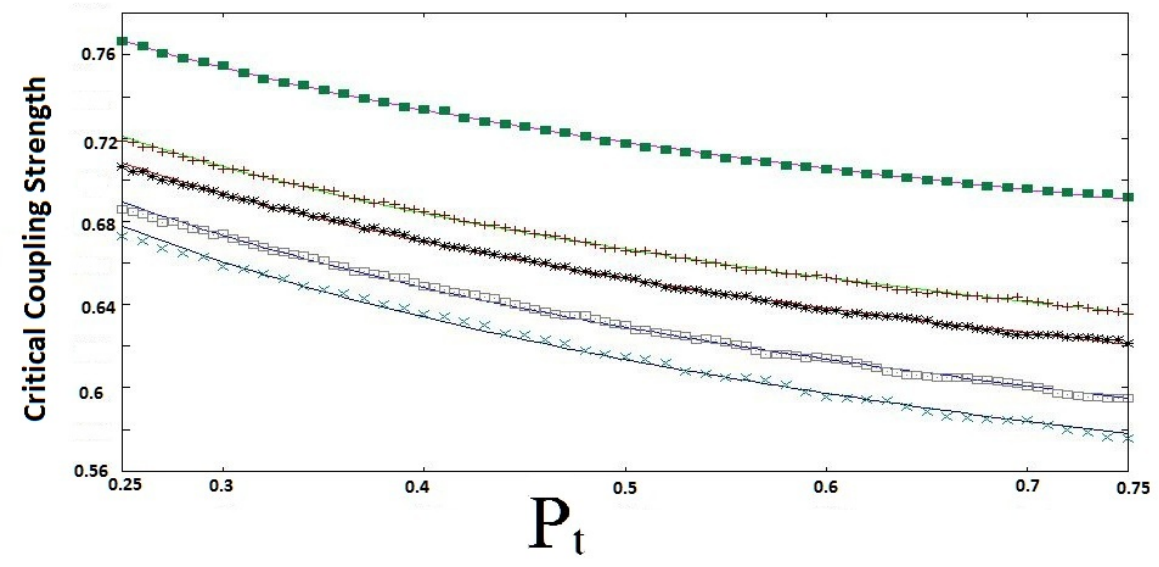

Figure 1.4: Variation of the average critical coupling strength $\langle \epsilon_c \rangle$ on the probability of link change p_t, for fraction of random links p_s equal to (from top to bottom): 0.5; 0.65; 0.7; 0.8; 0.9.

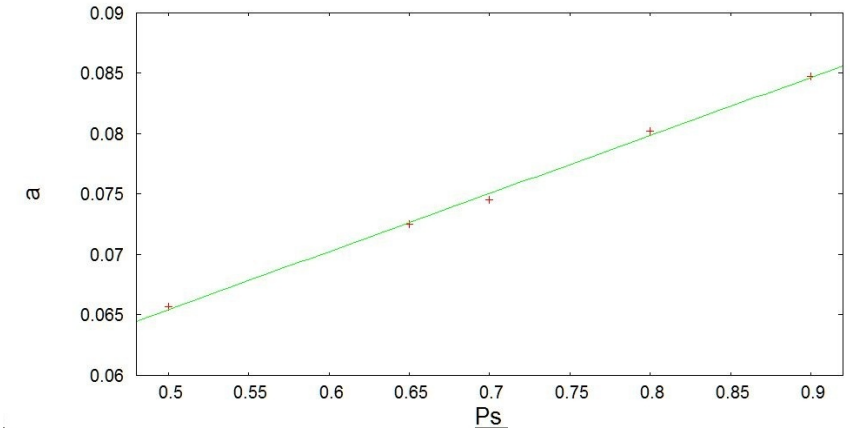

Figure 1.5: Plot of parameter a (see Eqn. 1.3) vs p_t. The best fit line has slope equal to 0.0480409 (with standard deviation equal to 2.764%) and intercept equal to 0.0413957 (with standard deviation equal to 2.319%)

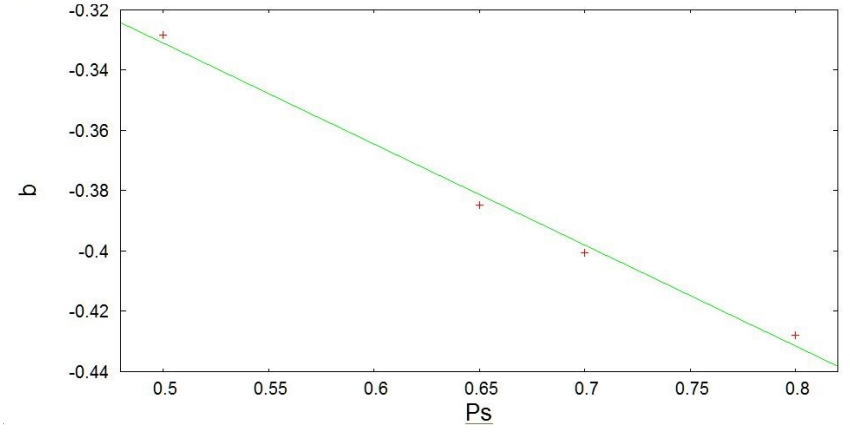

Figure 1.6: Plot of parameter b (see Eqn. 1.3) vs p_t. The best fit line has slope equal to 0.334595 (with standard deviation equal to 6.018%) and intercept equal to 0.0413957 (with standard deviation equal to 8.25%)

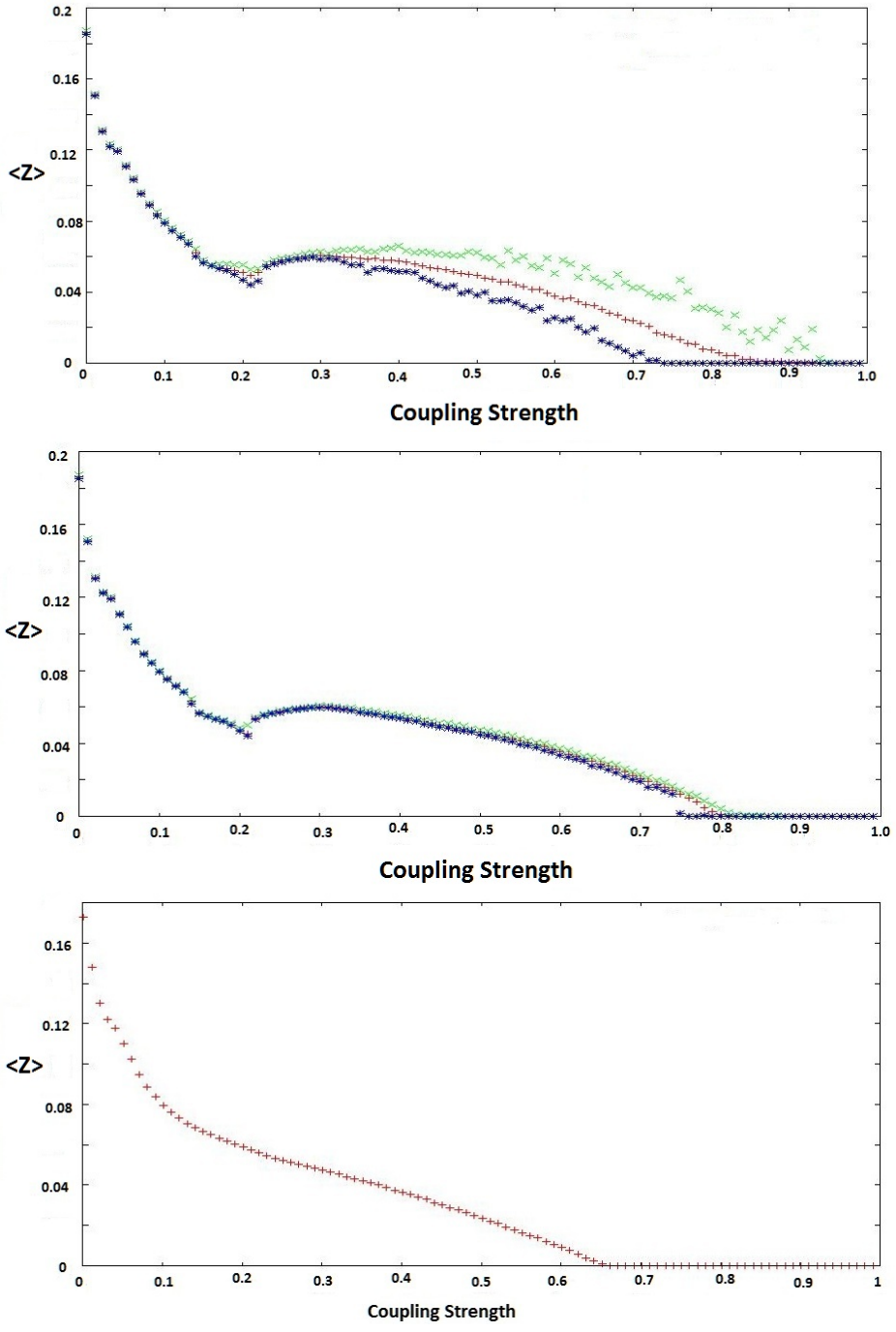

Figure 1.7: variation of the averaged synchronization error $\langle Z \rangle$ (in red), the maximum synchronization error Z_{max} (in green), the minimum synchronization error Z_{min} (in blue) as a function of coupling strength ϵ, for $p_t = 0$ (i.e. a static network) [top]; $p_t = 0.01$ [middle]; $p_t = 0.5$ [bottom].

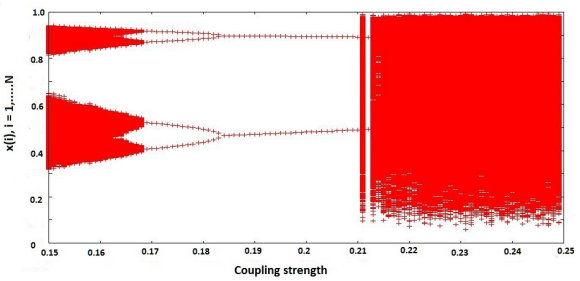

Figure 1.8: Bifurcation diagram showing the state of the system $x_n(i), i = 1, \ldots N$, for a system of size $N = 50$, with respect to coupling strength ϵ.

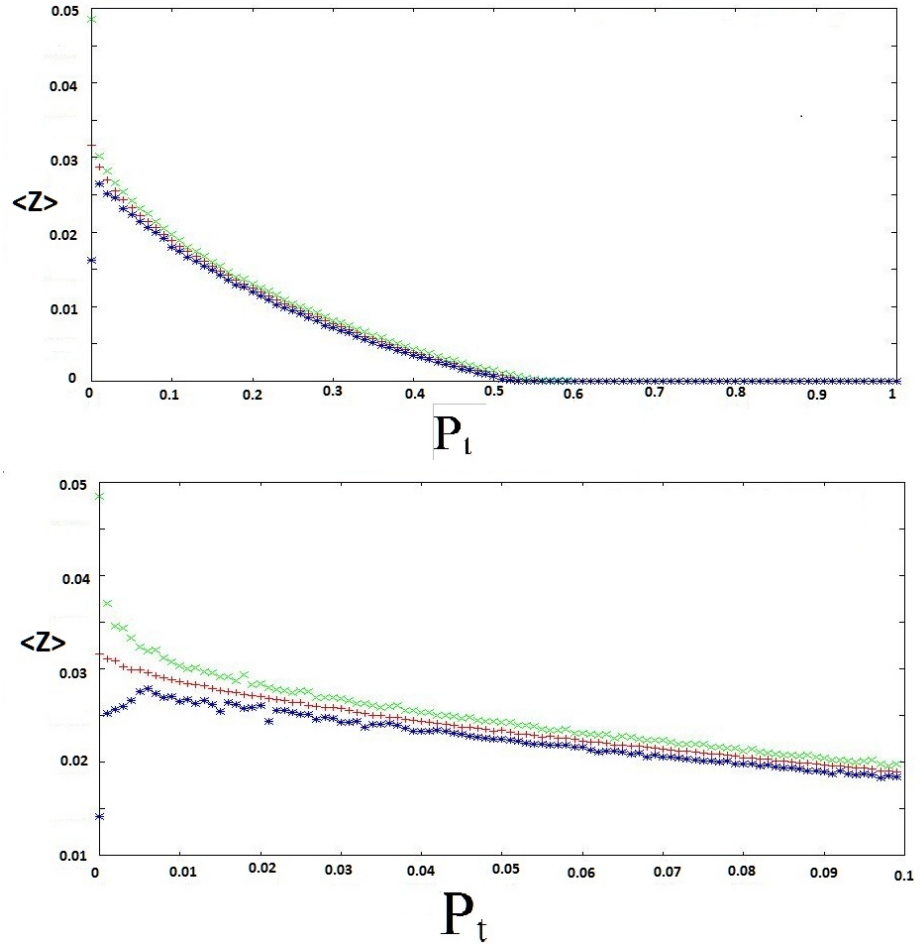

Figure 1.9: variation of the averaged synchronization error $\langle Z \rangle$ (in red), the maximum synchronization error Z_{max} (in green), the minimum synchronization error Z_{min} (in blue) as a function of p_t, for $\epsilon = 0.65$.

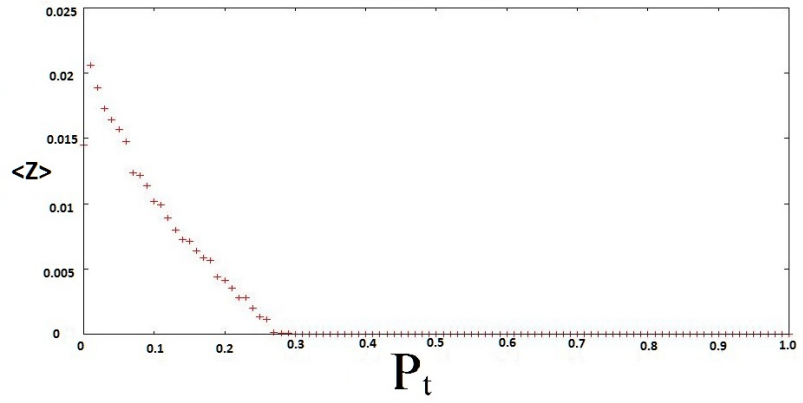

Figure 1.10: variation of the averaged synchronization error $\langle Z \rangle$ (in red), the maximum synchronization error Z_{max} (in green), the minimum synchronization error Z_{min} (in blue) as a function of p_t, for $\epsilon = 0.7$.

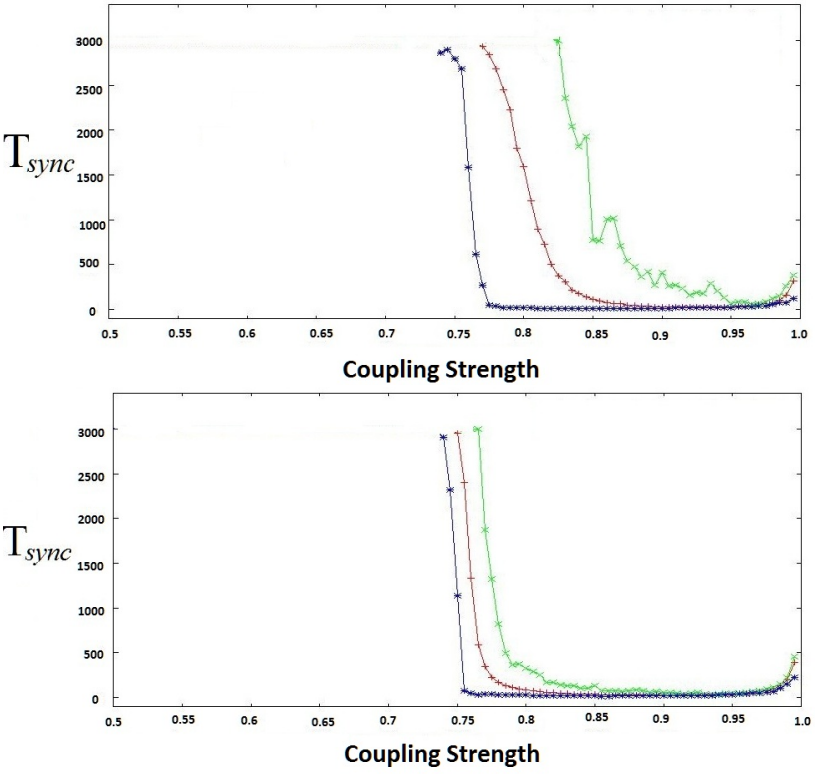

Figure 1.11: Variation of the average time needed to reach the synchronized state $\langle T_{sync} \rangle$, the maximum time $T_{syncmax}$ and minimum time $T_{syncmin}$ with respect to coupling strength ϵ. To calculate $\langle T_{sync} \rangle$ we average over 3000 time steps and 500 different initial conditions. Here the size of the system is $N = 50$, $p_s = 0.65$, and $p_t = 0.01$ [top]; $p_t = 0.1$ [bottom].

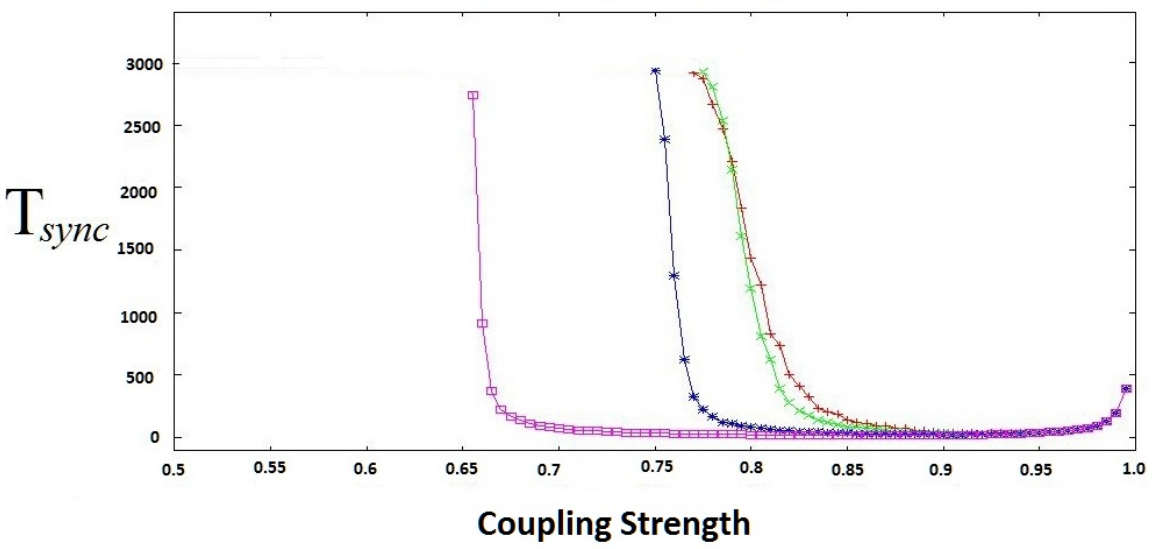

Figure 1.12: Variation of the average time needed to reach the synchronized state $\langle T_{sync} \rangle$ the maximum time $T_{syncmax}$ and minimum time $T_{syncmin}$ with respect to coupling strength ϵ.. To calculate $\langle T_{sync} \rangle$ we average over 3000 time steps and 500 different initial conditions. Here $p_s = 0.65$, $N = 50$ and $p_t = 0.01; 0.02; 0.1; 0.5$.

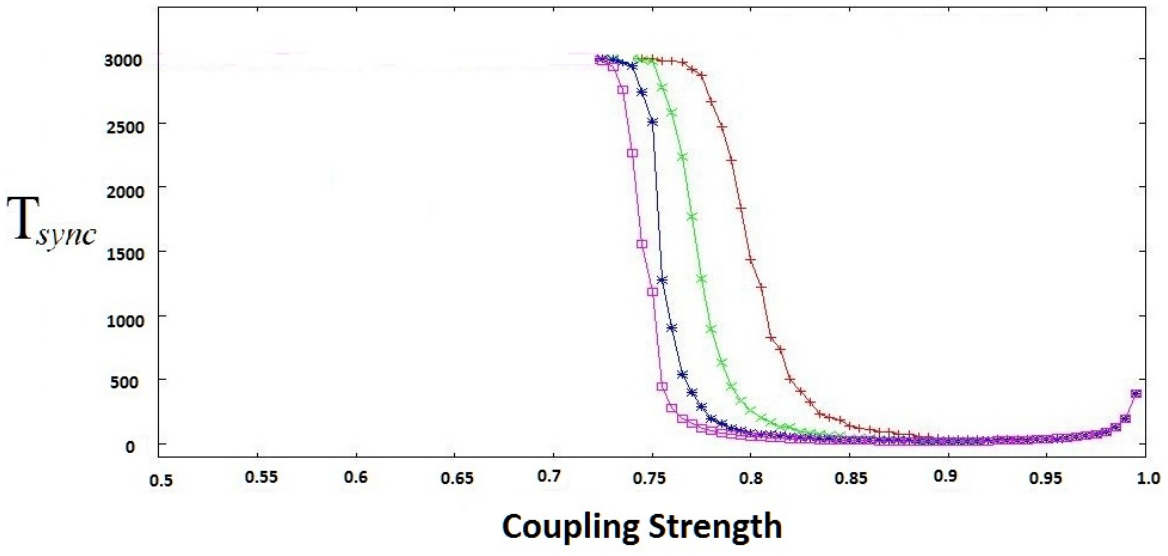

Figure 1.13: Variation of the average time needed to reach the synchronized state $\langle T_{sync} \rangle$, with respect to coupling strength ϵ. To calculate $\langle T_{sync} \rangle$ we average over 3000 time steps and 500 different initial conditions. Here $N = 50$, $p_t = 0.01$, and $p_s = 0.65, 0.75, 0.85, 1.0$.

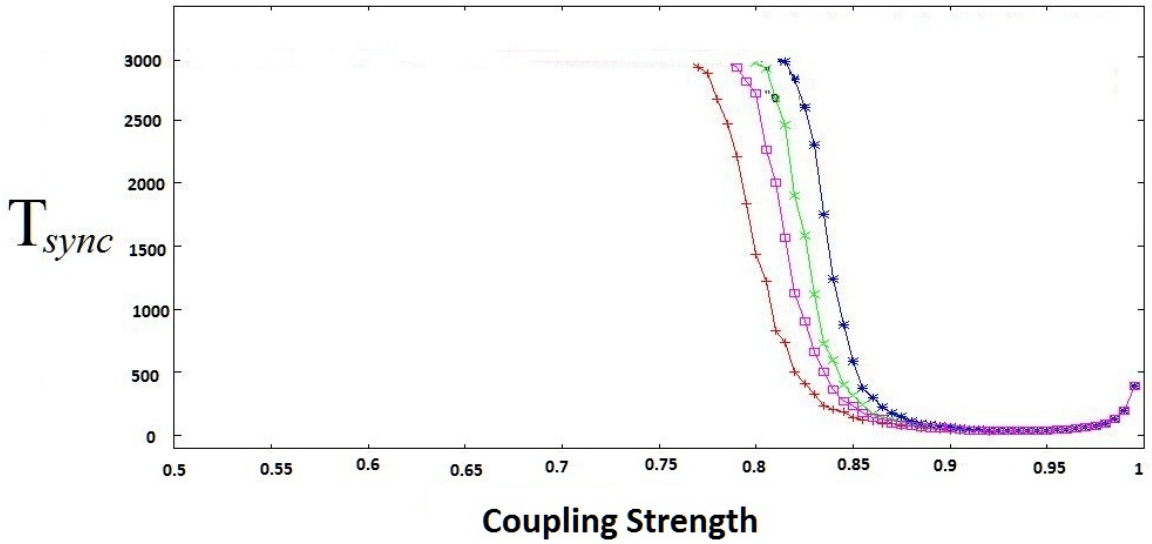

Figure 1.14: Variation of the average time needed to reach the synchronized state $\langle T_{sync} \rangle$, with respect to coupling strength ϵ. To calculate $\langle T_{sync} \rangle$ we average over 3000 time steps and 500 different initial conditions. Here $p_t = 0.01$, $p_s = 0.65$ and $N = 50, 75, 100, 150$.

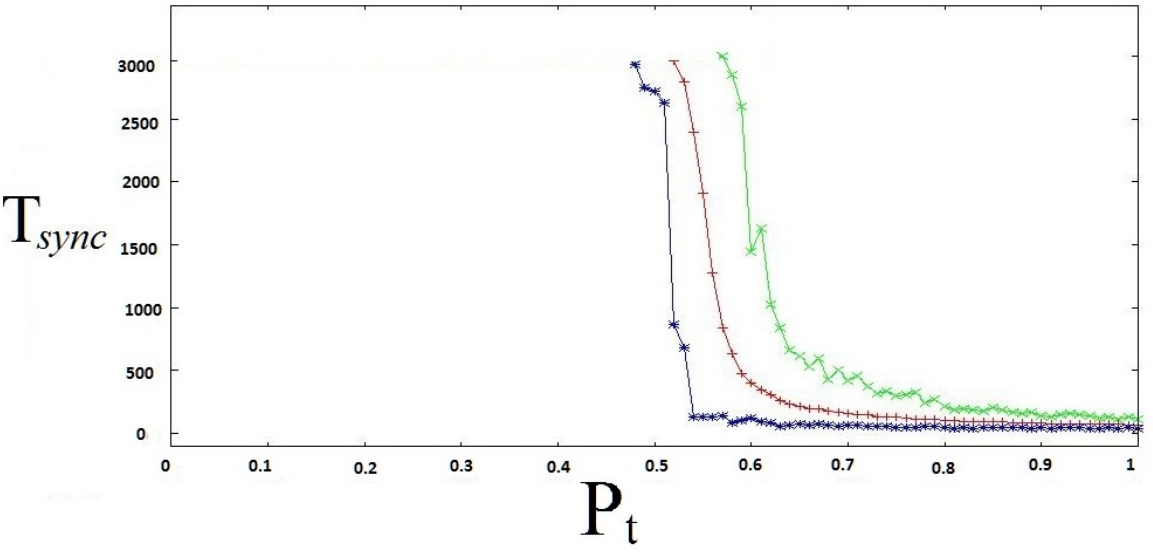

Figure 1.15: Variation of the average time needed to reach the synchronized state $\langle T_{sync} \rangle$, the maximum time $T_{syncmax}$ and minimum time $T_{syncmin}$ with respect to probability p_t of link change. To calculate $\langle T_{sync} \rangle$ we average over 3000 time steps and 500 different initial conditions. Here $\epsilon = 0.65$, $p_s = 0.65$.

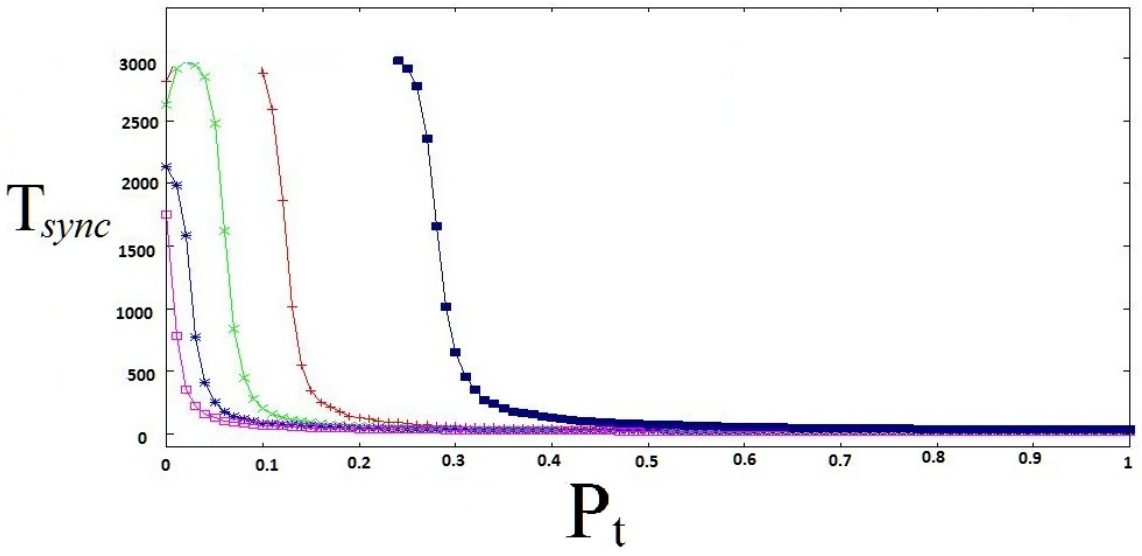

Figure 1.16: Variation of the average time needed to reach the synchronized state $\langle T_{sync} \rangle$, with respect to probability p_t of link change. To calculate $\langle T_{sync} \rangle$ we average over 3000 time steps and 500 different initial conditions. Here $\epsilon = 0.75$, $N = 50$; $p_s = 0.5, 0.65, 0.75, 0.85, 1.0$.

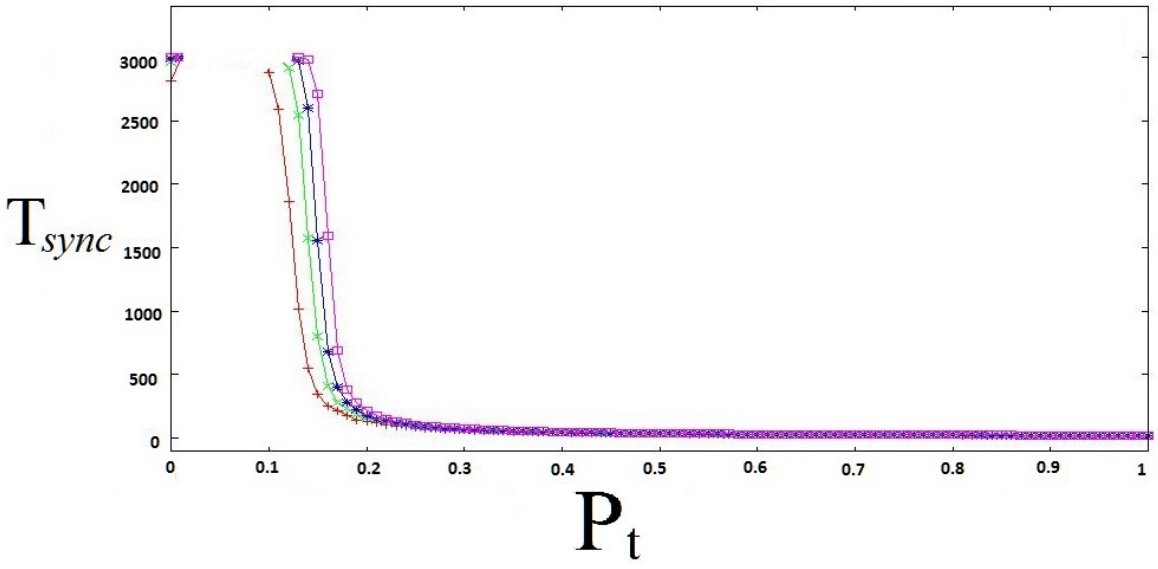

Figure 1.17: Variation of the average time needed to reach the synchronized state $\langle T_{sync} \rangle$, with respect to probability p_t of link change. To calculate $\langle T_{sync} \rangle$ we average over 3000 time steps and 500 different initial conditions. Here $\epsilon = 0.75$, $p_s = 0.65$; $N = 50, 75, 100, 150$.

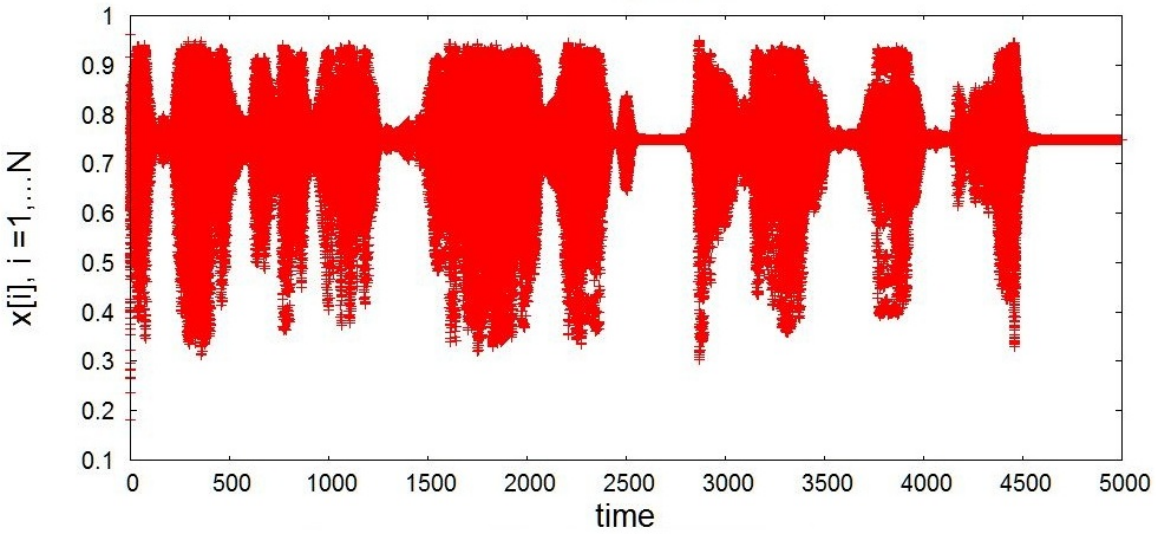

Figure 1.18: Time evolution of a system of coupled chaotic logistic maps, with $p_t = 0.01$, $p_s = 0.65$, $\epsilon = 0.78$ and $N = 50$.

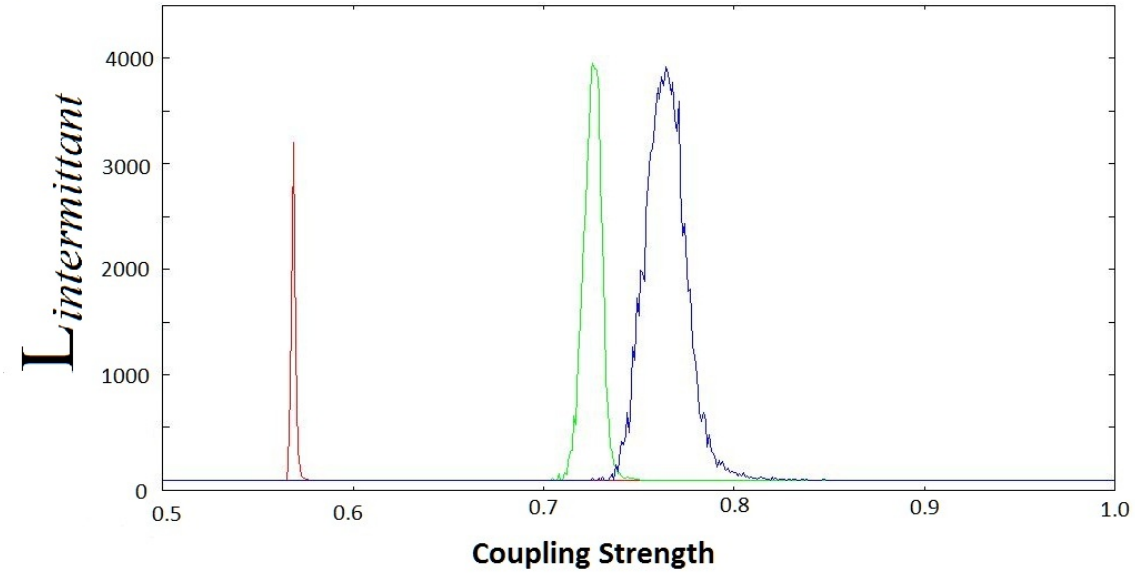

Figure 1.19: $L_{intermittant}$ vs. Coupling Strength for the case of local link changes, with fraction of random links $p_s = 0.8$, link switching probability $p_t = 0.01$(red); 0.1(green); 1.0(blue). Here network size N = 100, and $L_{intermittent}$ is obtained by aver- aging over 100 realizations.

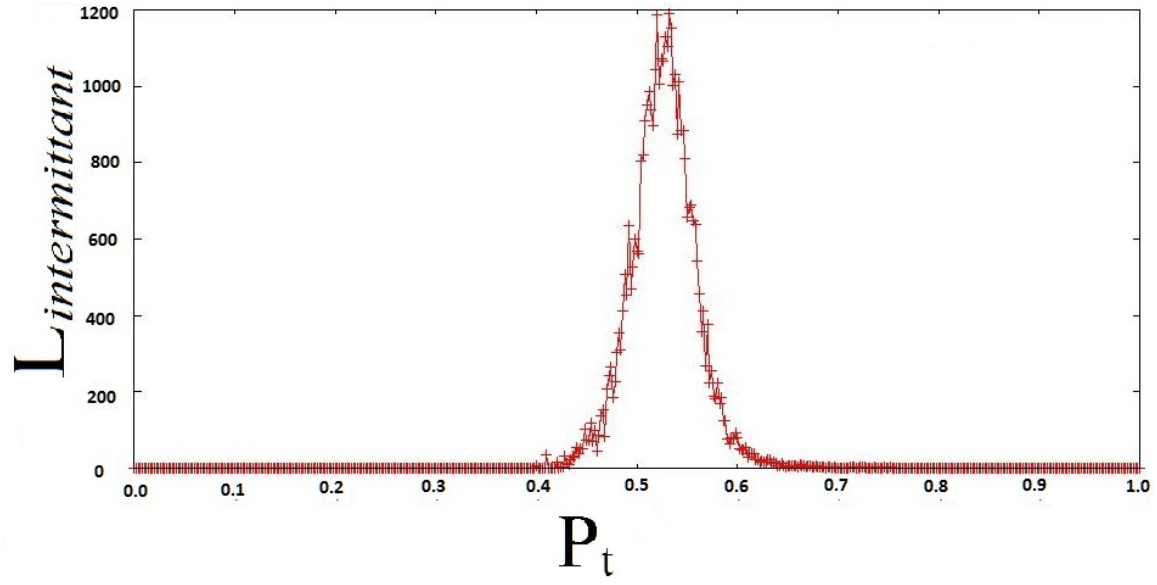

Figure 1.20: $L_{intermittant}$ with respect to the probaility p_t of link change, for a system of size $N = 50$, with $p_s = 0.65$ and $\epsilon = 0.65$, averaged over 100 realizations and system followed up to 2000 iterations.

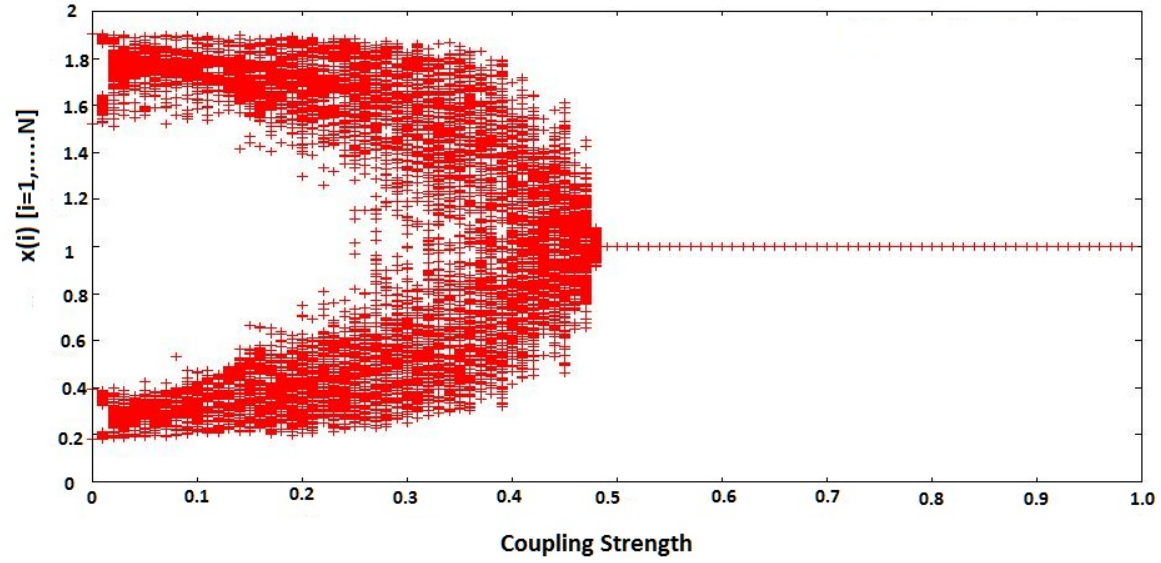

Figure 1.21: Variation of the state of the system $x_n(i)$ ($i = 1, \ldots, N$ and $n = 1, \ldots, 5$ after a transient time of 1000 iterations), with respect to coupling strength ϵ, at $p_t = 1.0$. The system size $N = 50$, and probability of spatial randomness p_s is 0.65.

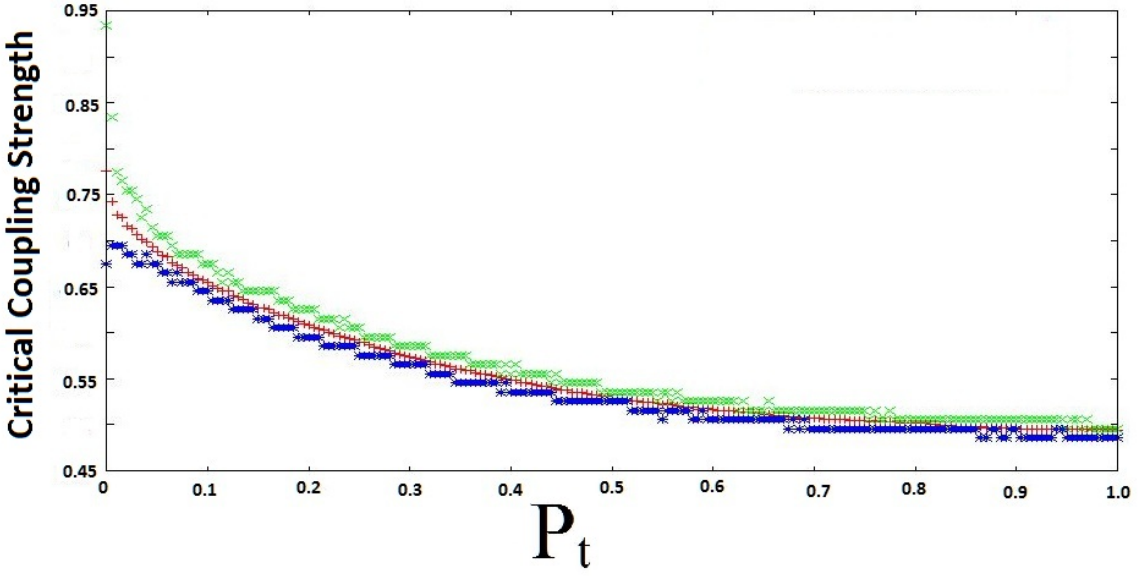

Figure 1.22: Variation of the average critical coupling strength necessary to obtain the synchronized state $\langle \epsilon_c \rangle$, the maximum coupling strength ϵ_{cmax} and the minimum coupling strength ϵ_{cmin}, with respect to probability p_t of link change. Here $p_s = 0.65$ and $N = 50$.

Chapter 2

A Cellular Automata Model of disease spread on a 2-Dimensional lattice

2.1 Introduction

How does a disease spread in a population? A question which has been greatly explored over the years. Various cases of epidemics and their phenomenological descriptions have been studied by the scientists.[18, 19, 20]

Mathematically, epidemiological models have been given to understand the dynamics of infectious disease.[21, 22] In a paper by Hethcote (1976) a well known model for disease progression: the SIRS cycle is explained. This model fits appropriately for diseases such as small pox, tetanus, influenza , typhoid fever and cholera[23]. Recently, a study by Ozcaglar (2012) has provided a review of earlier study on modeling different aspects of tuberculosis dynamics.[24]

Here in this work we focus on disease progression described by cellular automata model of SIRS cycle. Based on this model, work has been done previously to study the spread of infection within a population where the interactions are described by small world network.[25, 26, 27]

Rhodes and Anderson (1996) presented a lattice-based epidemic model of a non-fatal communicable disease in a mobile host population in which they observed novel dynamical behaviour.[28]

In this work we consider a lattice-based epidemic model where the population is represented by a 2-D lattice with the nodes representing the individuals and the individual follow the SIRS cycle of disease progression.

2.2 Model

We consider a population spread to be represented by a 2-D lattice of dimensions (MxN), where every node has 4 neighbors and with open boundaries. We further consider at the individual level the disease progresses in accordance with the well-known epidemiological model : *the SIRS cycle.*

The SIRS cycle can be elaborated in following steps : at the outset an individual is *susceptible* to infection (a stage denoted by S); on infection with other infected people, the individual moves to *infectious* stage (I). This is followed by a *refractory* stage (R), in this stage the individual becomes immune to disease and also does not infect others. But this immunity is temporary as the individual becomes susceptible again after some time interval.[27] Here, we impose a condition that *a susceptible(S) will become infected(I) if one or more of any of its neighbours is infected.*

Mathematically, the model is explained as follows:

Time is taken in discrete steps. Each element is characterized by a time counter τ_{ij}(t) = 0,1,.....τ_I + τ_R = τ_0, describing its phase in the cycle of the disease.[25] So at any time *t*,

if τ_{ij}(t) = 0 , then individual at site *(i,j)* is susceptible,

if $1 \leq \tau_{ij}(t) \leq \tau_I$ then it is infected and

if $\tau_{ij}(t) > \tau_I$ it is in refractory stage.

For, $\tau_{ij}(t) \neq 0$ the dynamics is given by $\tau_{ij}(t+1) = \tau_{ij}(t) + 1$, but when the cycle reaches the end the individual becomes susceptible again which means if $\tau_{ij}(t) = \tau_0$ then, $\tau_{ij}(t+1) = 0$.

Condition for infection:

Further, if $\tau_{ij}(t) = 0$, (the idividual is susceptible), then $\tau_{ij}(t+1) = 1$, if $1 \leq \tau_{xy}(t) \leq \tau_I$ where $xy \in \{(i-1,j);(i+1,j);(i,j-1);(i,j+1)\}$ which means the idividual becomes infected if one or more of its nearest neighbours is infected.

2.3 Infection Spread: How it actually looks in time?

We consider different initial configurations of the 2-D lattice. Then, based on the above explained model we studied the spread of infection and observed the changes in the state of individuals in the poplulation with time. This was done through a simple visual study of the 2-D lattice.

We fixed the parameters to be;

$\tau_I = 4$; $\tau_R = 9$; $\tau_0 = 13$ and lattice-size = 100x100.

The various senarios that we explored are as follows:

- **All individuals are susceptible to infection**. [$\tau_{ij} = 0$]

- **Case 1:** 1 infected individual at the center of the lattice.[$\tau_{50,50} = 1$]. This can be thought of as a control for this analysis as the results of this case can be intuitively understood.
  Fig. 2.1, exhibits that as time progresses the infection starts from the central seed and spreads symmetrically. At the individual level the disease cycle also progresses and so the phase of dynamical unit changes with time.
  The interaction of susceptible individuals with the infected ones is a key factor in the infection spread. As it takes place only at the outer boundary of the pattern so the infection ultimately gets removed from the population.
- **Case 2:** 1 infected individual at the center of the lattice (but permanently infected) [$\tau_{50,50} = 1$ always]. (Fig- 2.2) Same as the previous case, but a repeating pattern due to the permanent infection is seen.
- **Case 3:** 2 infected individuals at (50,25) & (50,75)) [$\tau_{50,25}$;$\tau_{50,75} = 1$]. From fig. 2.3 it can be clearly seen that even if the infection arising from one location interact with an other infection, the result is a symmetrical pattern.
- **Case 4:** 2 individual always infected and located symmetrically at (50,25) & (50,75)) [$\tau_{50,25}$;$\tau_{50,75} = 1$](Fig- 2.4).

After the control study, we now incorporate our model on a rather realistic case by introducing randomness to the initial configuration of the 2-D lattice.

- **Individuals are randomly distributed as susceptible with [$\tau_{ij} = \tau_S = 0$], their fraction is represented by S_0 and as refractory with $\tau_{ij} = \tau_R = (\tau_I + 1)$, their fraction is represented by R_0.**
  1 infected individual at the center of the lattice [$\tau_{50,50} = 1$], (S_0: 0.5; R_0: 0.5).
  Fig 2.5 shows interesting results, the infection was only initial but as time progressed a continuosly emerging infection pattern is seen.

For this case,a show-reel of infection spread
Time : t=0 to t=35 . (Zoomed in the center).

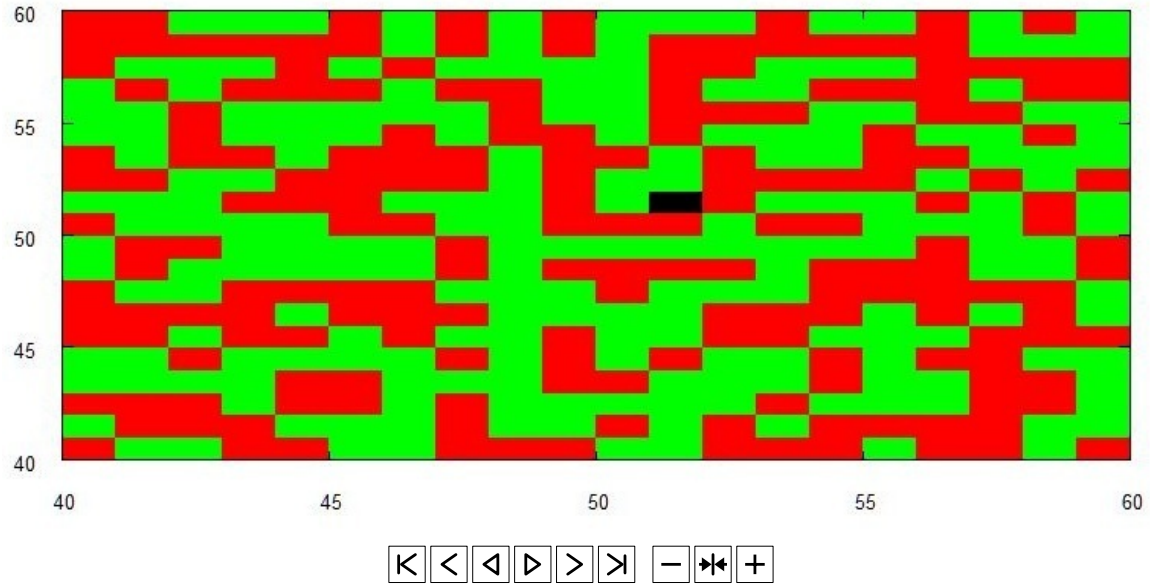

Similar results were obtained for the case when the individuals in R phase (τ_R) will have a randomly chosen phase from $[(\tau_I + 1), \tau_0]$.

2.4 Quantifying the infection in the population

Next, we discuss the possibility of quantifying the spread of infection in the population. For this we define a parameter I_t which represents the fraction of infected individual in the population at time *'t'*.

$$I_t = \frac{\text{Total number of infected individuals}}{\text{Total number of individuals}} \tag{2.1}$$

Similarly we also define S_0 and R_0 to be the initial fraction of Susceptible and Refractory individuals respectively.

An important observation from the visual study was that not always does one see infection being sustained in the population. Meaning, for a lot of cases the infection gets removed entirely from the population with time.

The infection spread depends on infected individual coming in contact with a susceptible individual. So, for a random initial configuration of S-R population the infection can either progress or not.

2.4.1 Histogram analysis

As per the above defined parameter, non-zero I_t will signify that infection stays in the population. At this point an analysis is required that gives an idea about the frequency of such non-zero I_t events. Fig- 2.6, shows the histogram analysis for 2 configuration [S_0:R_0

- 0.5:0.5] (top) & [S_0:R_0 - 0.75:0.25] and clearly it can be seen that a non-zero frequency is observed only around 2 region in I_t. So, if $I_t = 0$, then infection gets removed from the population. Also, if the infection do stays in the population with time ($I_t \neq 0$), then a small range for non-zero I_t signifies that to a great extent the spread pattern for different realizations remains the same.

2.4.2 Dependence of infection spreading on the fraction of susceptibles in the population

For fixed τ_I (4) and τ_0 (13) measurement of I_t (fraction of infect individuals on the lattice averaged over *'n'* realizations) were done for the complete range of S_0 (Initial fraction of susceptible individuals) [0,1]. This analysis gave insight about the influence of population type (distribution of susceptible and refractory individuals) on infection spread. Two major methods of defining the initial state/phase of individuals in the lattice were employed. In both the methods, the initial phase of 'S' population was $\tau_{ij} = 0$, but the 'R' population can be assumed to exist in following ways:

- Same phase($\tau_{ij} = \tau_I + 1$).
- Randomly different phase(τ_{ij} = randomly chosen from [$\tau_I + 1$,τ_0]).

Fig - 2.7, shows the variation of I_t with initial S_0 for the two cases discussed above.

2.4.3 Presenting the arguments to rationalize broad trends

In this section we discuss the broad trends seen in this study. The fig.2.8 shows the variation of I_t (fraction of infected individuals) over the whole range of S_0 (Initial fraction of Susceptible individuals in the population).Here, the key assumption taken in the analysis is that all the individuals in refractory period initially would have same phase ($\tau_R = \tau_I + 1 = 5$).

As seen clearly, I_t remains zero at low S_0 in the range $\approx$ (0,0.15) and also near $S_0 \approx 1$. For the in between range one see a continuously increasing and then decreasing trend which peaks around $S_0 \approx 0.65$. The spread of infection depends on basic level on infected individuals being in contact of a susceptible one, so it can be reasoned that at low S_0 the chances of this is fairly low so asymtotically the infection eventually gets removed from the population. When there are reasonable number of susceptible individuals in the population, it is seen that asymtotically infection stays in the population. The increasing trend in the range S_0 : (0.15,0.65) gives an indication that more and more realizations (initial population conditions) are now leading to infection spread. The maxima of this variation comes around a value $I_t \approx 0.25$, which is fairly close to 0.28 value we found out in the histogram analysis (this is the value of I_t observed for a realization leading to infection spread asymtotically).

It means that a great number of realizations are resulting in infection spread.
A decreasing trend in the value of I_t is seen at higher S_0 from here on which ultimately goes to zero near Initial $S_0 = 1$. The colored plots shown in the beginning gives a better idea about this kind of situation. Consider the case where initially all the individuals are susceptible to the infection and an individual in the center is infected, here one can see that the infection does spread but ultimately gets removed from the population. Also, the animation shown in the beginning clearly indicates the need of refractory indivduals in the spreading of infection. When there are not many refractory individuals that complete there cycle to again become susceptible, the infection does spread but asymtotically it will get removed and this infection process will not be repeated.
Hence, it can be said that for the infection to stay in the population a well mixed population is required with reasonable number of both susceptible and refractory individuals.

2.4.4 Checking the consistency of results

Different lattice sizes

It is important to check whether these results depend on the lattice size. From Fig- 2.9 it is clear that the size of lattice does not influence the infection spread both qualitatively and quantitatively.

Time-averaging results

Also the results obtained here are for a fixed time (t= 200). But, it becomes crucial to check the time averaged results for this model as the results may vary in time as well.
So, taking the time average for the range t = [200,300], with fixed τ_I (4) and τ_0 (13), infection seed at the center, 40x40 lattice ,and same phase ($\tau_{ij} = \tau_I + 1$) for Refractory fraction of population.
From 2.10, it is clear that even on time averaging the variation curve is showing the same trend, hence the analysis at a particular time yields same results as that with time average.

Random Infection seed

Another essential component of this analysis would be the location of initial infection seed. Since, it is the source of disease spread it becomes necessary to check the validilty of these results for a random initial infection.
Fig -2.11, clearly points out that a random infection seed only changes the origin of the pattern. From fig - 2.12, 2.13 it can be seen that if the infection seed is random present at any position in the lattice, the variation of I_t over the range of S_0 remains qualitatively same as that for infection seed at center of the lattice. Also, I_t remains invariant even in this situation, shown in Fig- 2.14.

2.4.5 Dependence on the dynamical characteristics of the disease cycle(τ_I; τ_R; τ_0)

The SIRS cycle itself plays a crucial role in the spread of the disease. The next part of analysis focus on this interplay between the SIRS cycle and infection spread. According to our model, out of three compartments of SIRS cycle, susceptible is fixed (τ_S =0), but the other two can be changed. And taking different τ_I and τ_R, the infection spread analysis was done.

Fig. 2.15 shows that when a infection spreads the pattern formed is similar looking although as the infection and refractory periods are different, one see quantitatively different pattern.

From Fig- 2.16 (exhibit the case when R population is having a fixed same phase) it is clearly seen that the variation of I_t with S_0 shows a high dependence on the ratio $\frac{\tau_I}{\tau_R}$. For a case when

$\frac{\tau_I}{\tau_R} < 1$ [$\tau_I = 4$, $\tau_R = 9$] & [$\tau_I = 4$, $\tau_R = 9$], a similar variation is observed with I_t zero at high and low $S_{fraction}$ and in between range forming a smooth peak. Here, a noteworthy point is even when the actual cycle length changes the variation curve does not changes much.

When, $\frac{\tau_I}{\tau_R} = 1$ [$\tau_I = 4$, $\tau_R = 4$] & [$\tau_I = 9$, $\tau_R = 9$] a symmetrical variation curve is seen and irespective of total cycle length, both lead to exactly same result, both qualitatively and quantitatively.

An interesting case arises when $\frac{\tau_I}{\tau_R} > 1$ [$\tau_I = 9$, $\tau_R = 4$], in this case one observe a high and constant I_t value for the lower range of S_0 upto $\approx .0.3$ and then it smoothly goes to zero as S_0 reaches 1.0.

The same analysis when done for the case of R population having randomly different phase is shown in Fig- 2.17. Here, it can be clearly seen that for fixed disease cycle length (τ_0 = 13) as the period of infection (τ_I) increases the slope of I_t vs. $S_{fraction}$ also increases. It indicates that for a population having individuals in random phases in disease cycle will qualitatively remains the same with changing infection period (τ_I), although the fraction of infected individuals would be greater for larger τ_I.

2.4.6 Changing the heterogeneity in the initial population

Here we have considered two basic initial configuration of population, namely R population having a fixed same phase and R population having randomly different phase. Now, consider a case where the population is in between these two cases, means the refractory individuals in the population are having phases neither completely random nor completely fixed to same value.

We adopt two methods to achieve such configuration:

- **Mixture of uniform and non-uniform sub-populations:** We define a parameter η which represents the fraction of R population having randomly different phases initially and similarly, we can also say that (1 - η) represents fraction of R population having a fixed phase initially ($\tau_R = \tau_I + 1$).
  Fig- 2.18 exhibits the change in the variation curve as η and hence the initial configuration changes. It can be clearly seen that as the transition takes place from one extremal initial condition (all R individuals in same phase) to the other (all R individuals in randomly different phases) the variation curve of I_t gradually changes its form.

- **Varying the range of phases:** We consider that the initial phase of individuals in R compartment of SIRS cycle can be any integer from the range χ. This range can be taken to be anything from [τ_I +1, τ_R] (completely random phases) to [τ_I +1, τ_I + 1] (completely fixed and same phase).

  First we perform the analysis by taking the range χ with fix lower bound τ_I +1 and different upper bounds. Fig- 2.19 exhibits the variation curves for different χ: [5,5]; [5,7]; [5,9]; [5,11]; [5,13]. It can be clearly seen that as the transition takes place from one extremal initial condition (all R individuals in same phase) to the other (all R individuals in randomly different phases) the variation curve of I_t gradually changes its form.

  Another way of altering the range χ would be to fix the upper bound at τ_R and take different lower bounds. Fig- 2.20 exhibits the variation curves for different χ: [5,13]; [7,13]; [9,13]. Here, shortening the range χ lead to decrease in I_t but the qualitatively the variation curve remains the same and for χ close to end of cycle I_t is zero in the entire S_0 range: [0,1]. Hence, we can conclude that when the initial phases of refractory individuals are taken more towards a value at the end of the disease cycle then infection gets removed from the population.

The above done analysis basically covers two distinct senarios where the refractory individuals initially have same phase and randomly different phases. A comparison can be done between the two by considering the randomly different phase situation with its mean at say, 9 (median of refractory period[5,13]) and the same phase situation at initial τ_R = 9. From fig.- 2.21, it can be seen that both these senarios are actually distinct, where the randomly different phase situation has the continuously decreasing variation curve and the same phase situation ($\tau_R = 9$) has a variation curve qualitatively similar to same phase with $\tau_R = 4$ but with considerably low I_t peaking at a lower value of S_0.

2.5 Discussions and Summary

Here we discuss broadly the model and its analysis by summarising the key ideas and results. Basesd on the cellular automata model of SIRS cycle disease progression[25] we considered a population represented by a 2-Dimensional lattice. Coupling was introduced in the system by putting the condition for infection that if an individual comes in contact with an infected individual then it will become infected.

To get an idea of the spread of infection visually we took different initial population senarios and observed with time how the state of individuals changes. We found out that for a completely susceptible population a infect does not give rise to permanent infection although the infection does spread but ultimately gets removed from the population. A permanent infection seed does lead to greater and permanent infection spread in the population. All of which was intuitively understandable, next we considered a situation where individuals are both in susceptible and refractory phase. Here, the population is randomly distributed and an interesting observation was that even for an infection seed put only initially one could see a permanent infection spread pattern.

Now, we quantified the infection spread by defining a parameter I_t which represented the fraction of infected individuals in the population. A key observation was that on fixing the fraction of suseptible and refractory individuals if we take different random realizations then not all realisations lead to permanent infection spread. Depending on the S_0 and R_0 the frequency of permanent infection spread also changes.

We next looked at the variation of I_t over the entire range of S_0, this was done for two senarios, for refractory individuals in same phase initially and in randomly diiferent phase. Contrasting trends were observed as for the randomly different phase a continuously decreasing trend was seen and for same phase situation a curve was seen which increased continuously and after a point starts to decrease continuously, at the extremes zero infection was observed.

The analysis done till now was at a particular time, so by taking a time average of I_t we checked that whether it is time dependent and the results of this analysis suggested that the trends here does not change with time. Also, we checked proved the consistency of the results for different lattice size and random infection seed situation.

The system here showed strong dependence on the disease cycle, the change in variation curve for different infection period indicated that for the situation where Refratory individuals are in same phase initially the ratio $\frac{\tau_I}{\tau_R}$ decides the trend qualitatively. Although for the situation where Refratory individuals are in randomly different phase initially only quantitative change occur in the variation curve.

Next we considered a more general senarios where the randomness in the phases of Refractory individuals is not complete. We took two approaches, in one case the randomness was changed by changing the fraction of individuals with randomly different phases in R and

other case was shortening the range of randomness in phases. Both theses analysis lead to the conclusion that the variation curve transitions from one case to other in a smooth fashion.

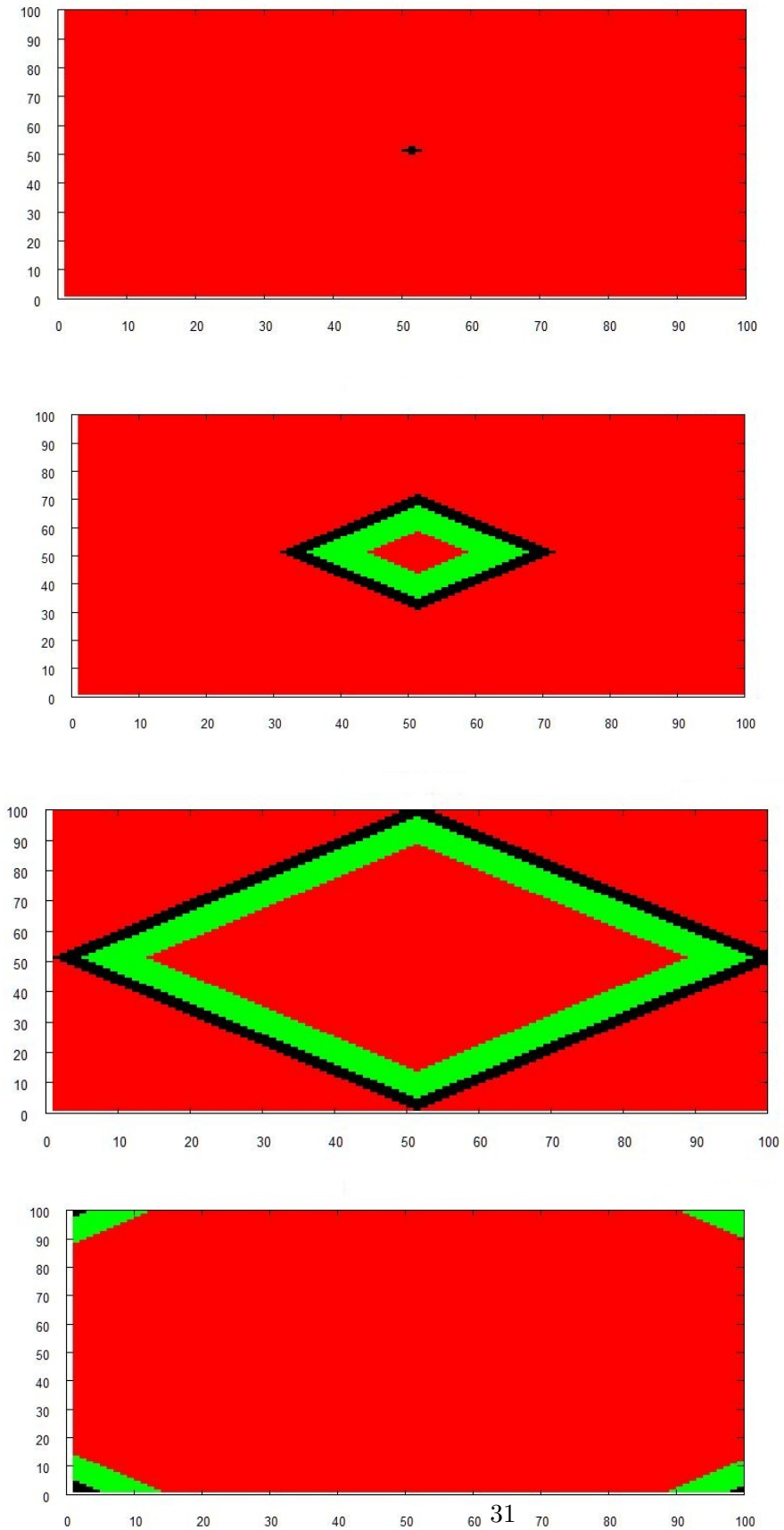

Figure 2.1: Snapshots of the infection spread pattern at different times; t= 1, 20, 50, 100. [color scheme: Green-refractory;Red-Susceptible;black-infected]

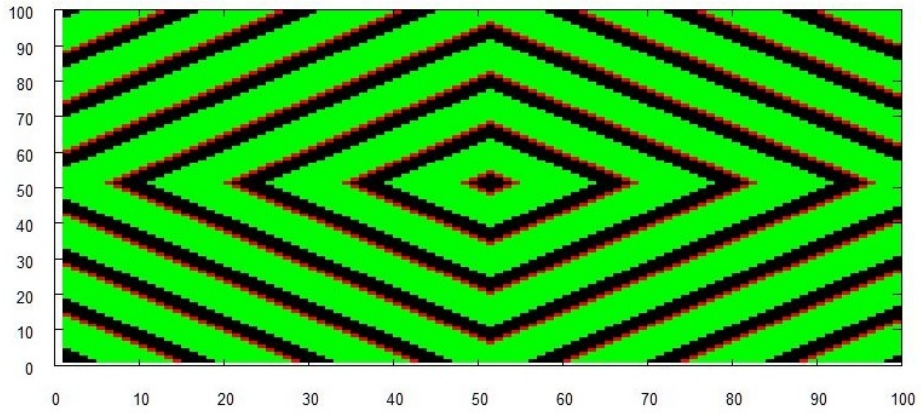

Figure 2.2: Snapshot of the infection spread pattern at time=100[color scheme: Green-refractory;Red-Susceptible;black-infected]

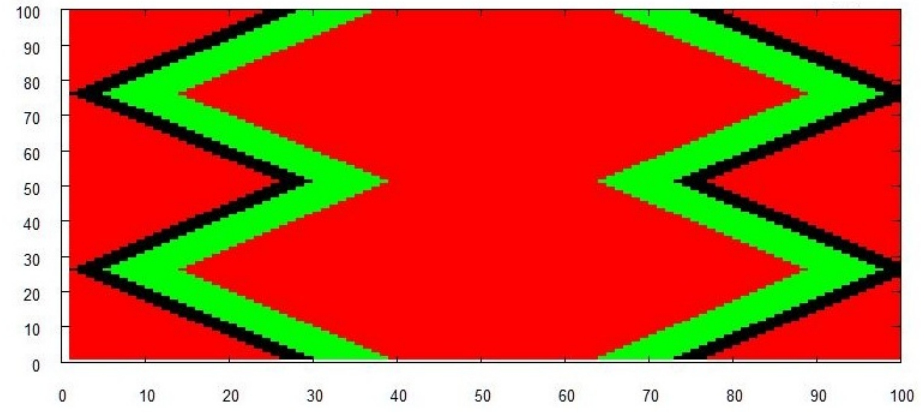

Figure 2.3: Snapshot of the infection spread pattern at time=50[color scheme: Green-refractory;Red-Susceptible;black-infected]

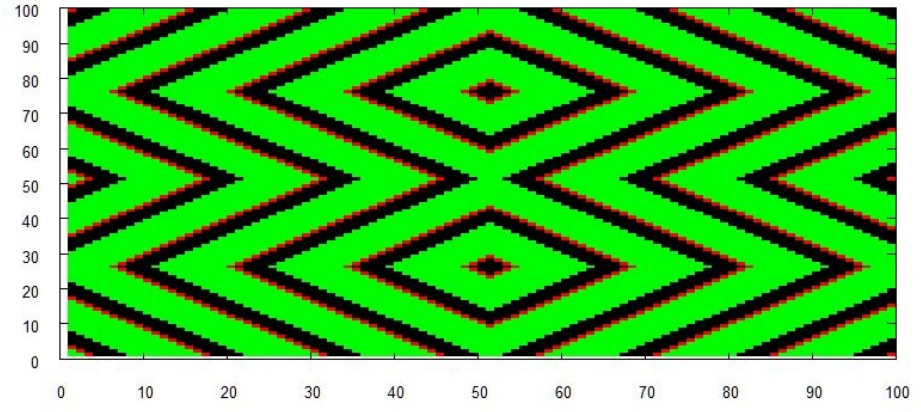

Figure 2.4: Snapshot of the infection spread pattern at time=100[color scheme: Green-refractory;Red-Susceptible;black-infected]

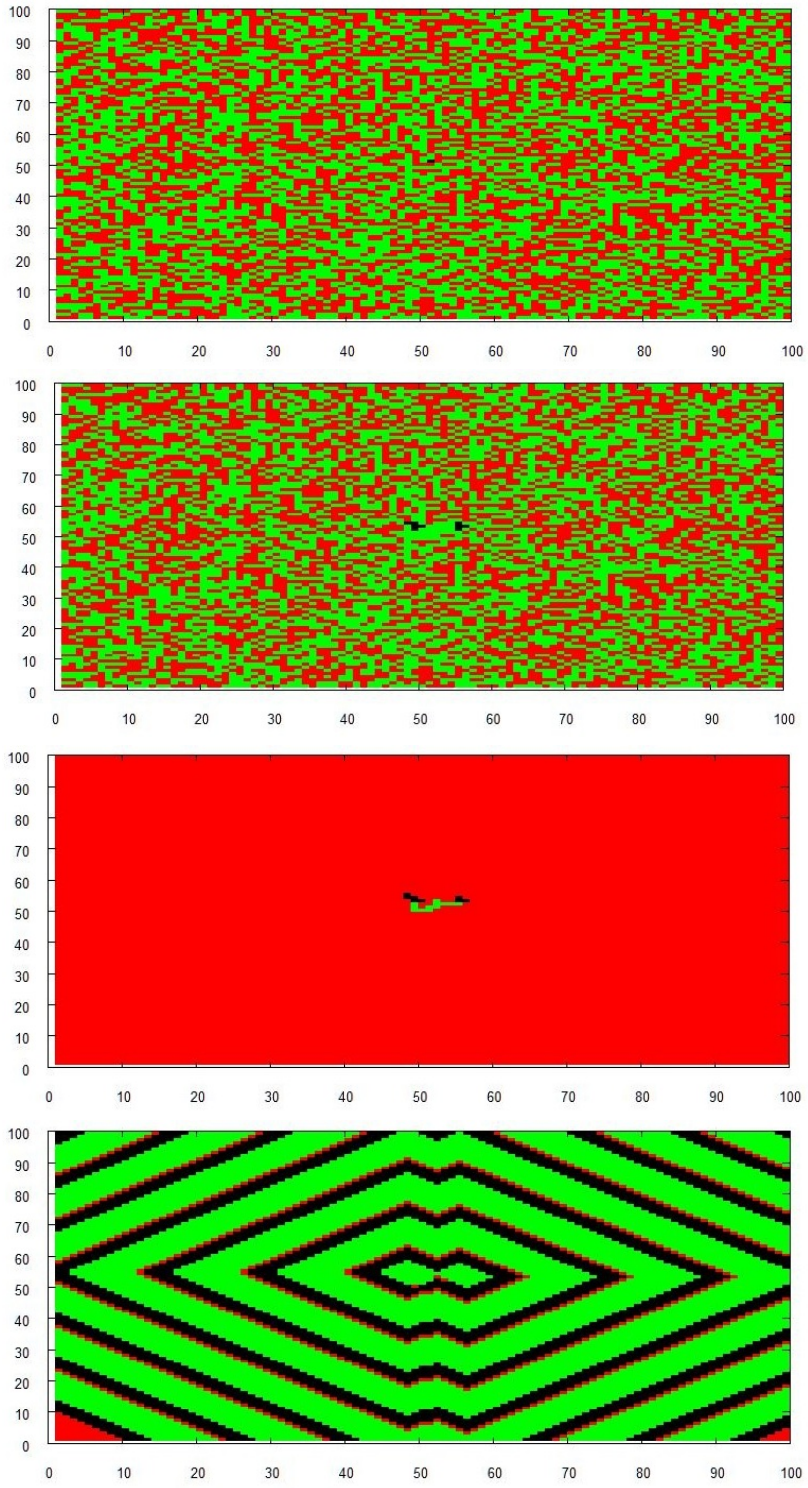

Figure 2.5: Snapshots of the infection spread pattern at time=0,5,8,9,20,100 (order-left to right & top to bottom)[color scheme: Green-refractory;Red-Susceptible;black-infected]

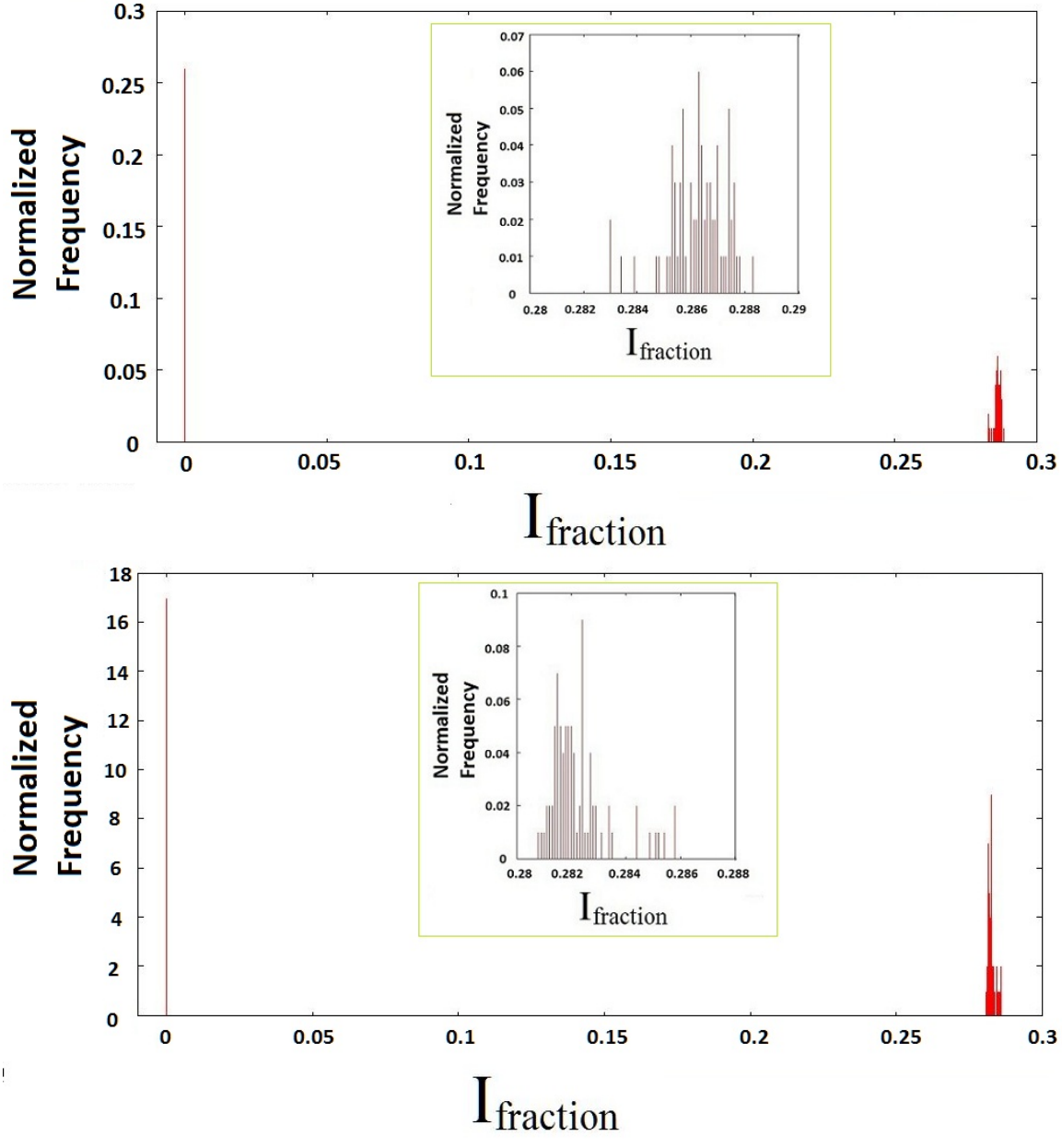

Figure 2.6: Histogram for I_t after t= 200 [S_0:R_0 - 0.5:0.5](top) & [S_0:R_0 - 0.75:0.25] ; initially infection put at the center with $\tau_I = 4$; $\tau_0 = 13$

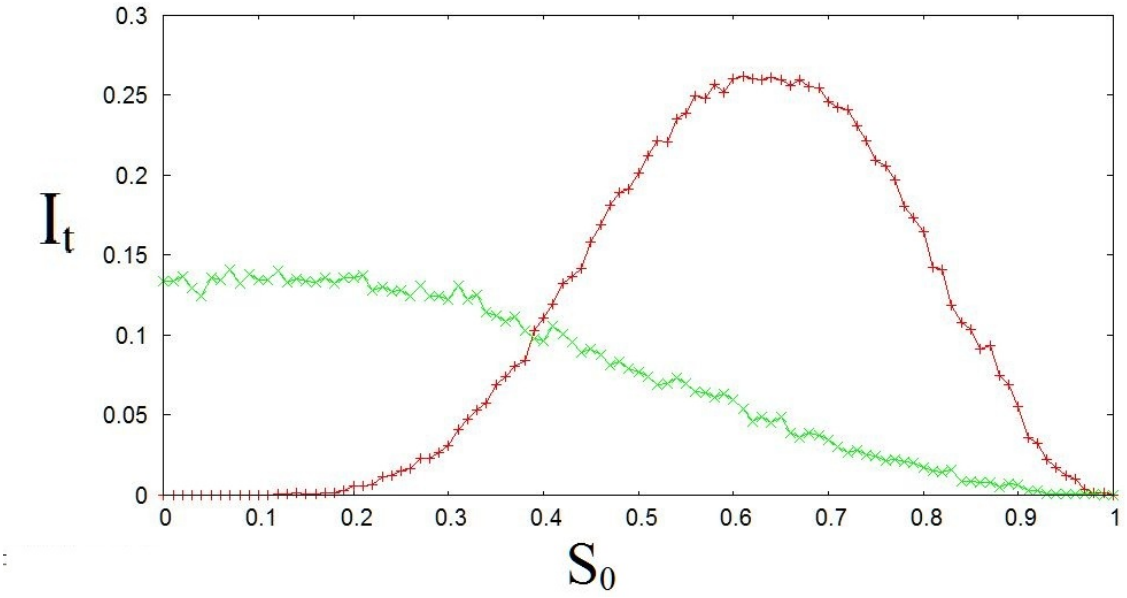

Figure 2.7: Variation of I_t (after t= 200) with S_0 (Red curve- R population with same phase; Green curve- R population with randomly different phase)[initially infection put at the center] N= 40x40; $\tau_I = 4$; $\tau_0 = 13$, averaged over 10^3 realizations.

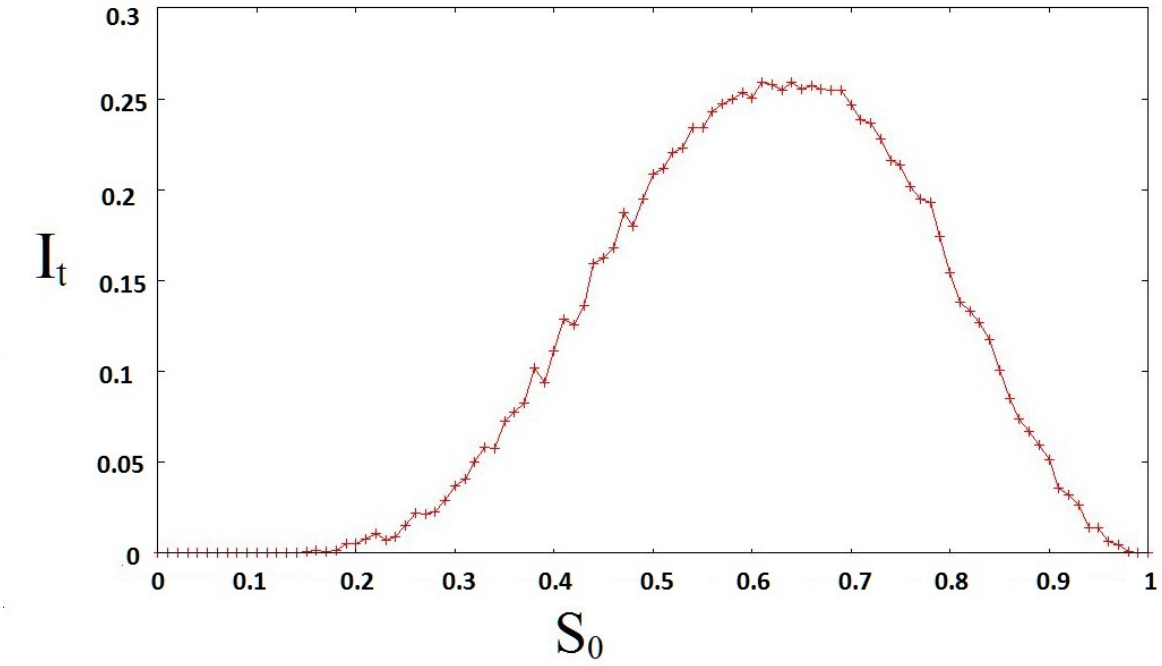

Figure 2.8: Variation of I_t (after t= 200) with S_0). Refractory population having same phase in R[$\tau_R = \tau_I + 1 = 5$]. $\tau_I = 4$, $\tau_R = 9$. N = 40x40.[initial infection at the center]. averaged over 10^3 realizations

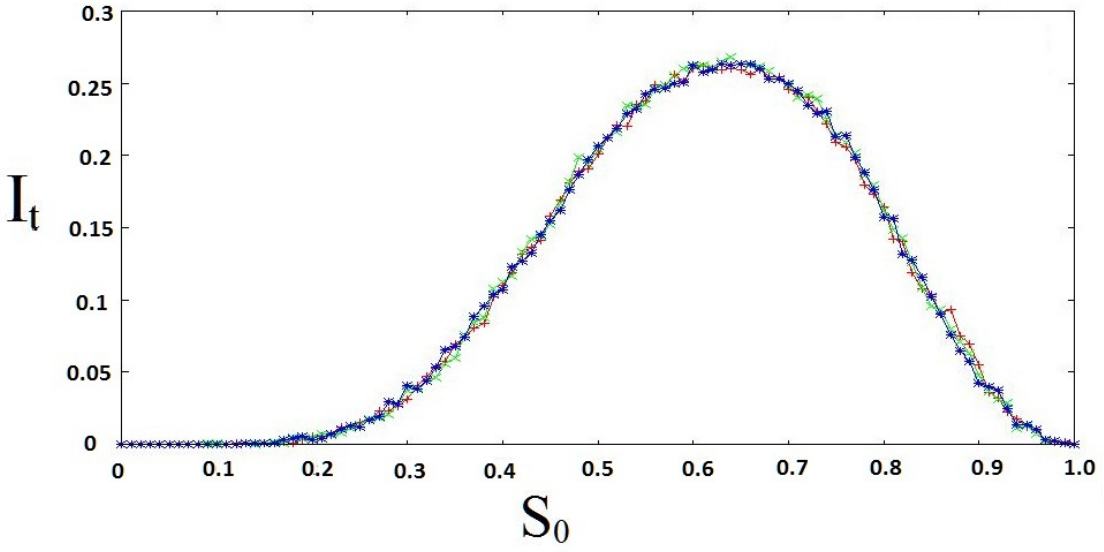

Figure 2.9: Variation of I_t (after t= 200) with S_0 for population having same phase in R. N = 40x40 (Red curve); 100x100 (Green curve); 70x70 (Blue curve)[initially infection put at the center] $\tau_I = 4$; $\tau_0 = 13$, averaged over 10^3 realizations.

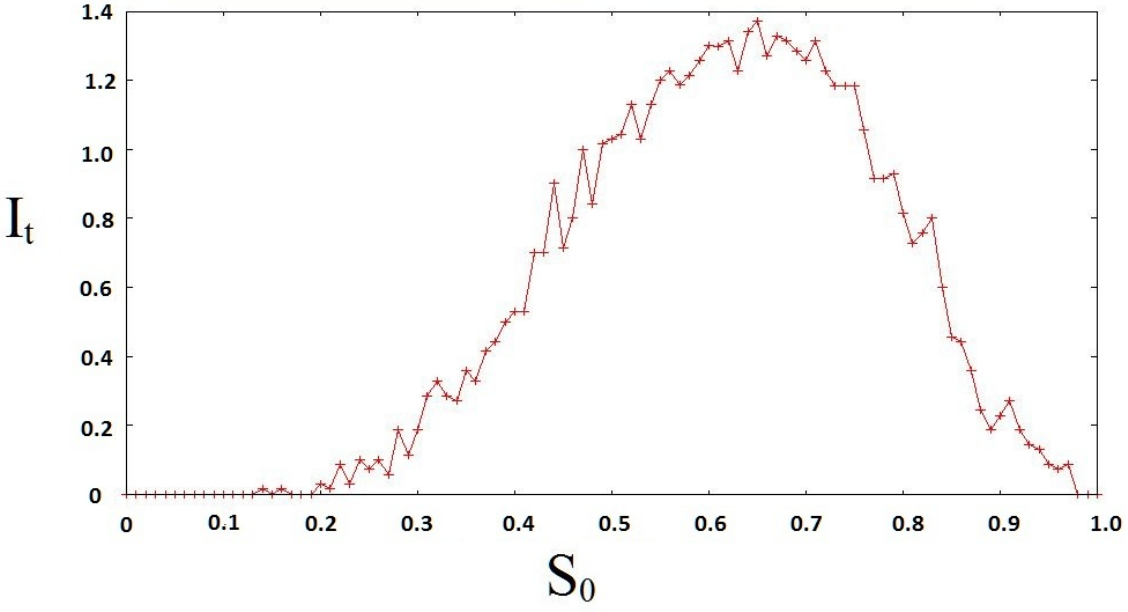

Figure 2.10: Variation of I_t (averaged over t= [200,300]) with S_0 for population having same phase in R. N = 40x40 [initially infection put at the center] $\tau_I = 4$; $\tau_0 = 13$, averaged over 10^3 realizations.

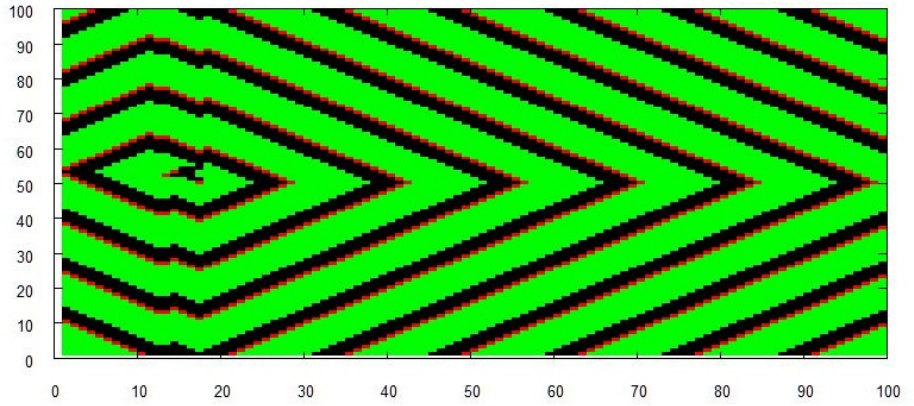

Figure 2.11: Snapshot of the infection spread pattern at t= 200 and initially infection at a random site with $\tau_I = 4$; $\tau_0 = 13$ and [S_0:$R_{fraction}$ - 0.5:0.5] [color scheme: Green-R; Red-S; black-I]

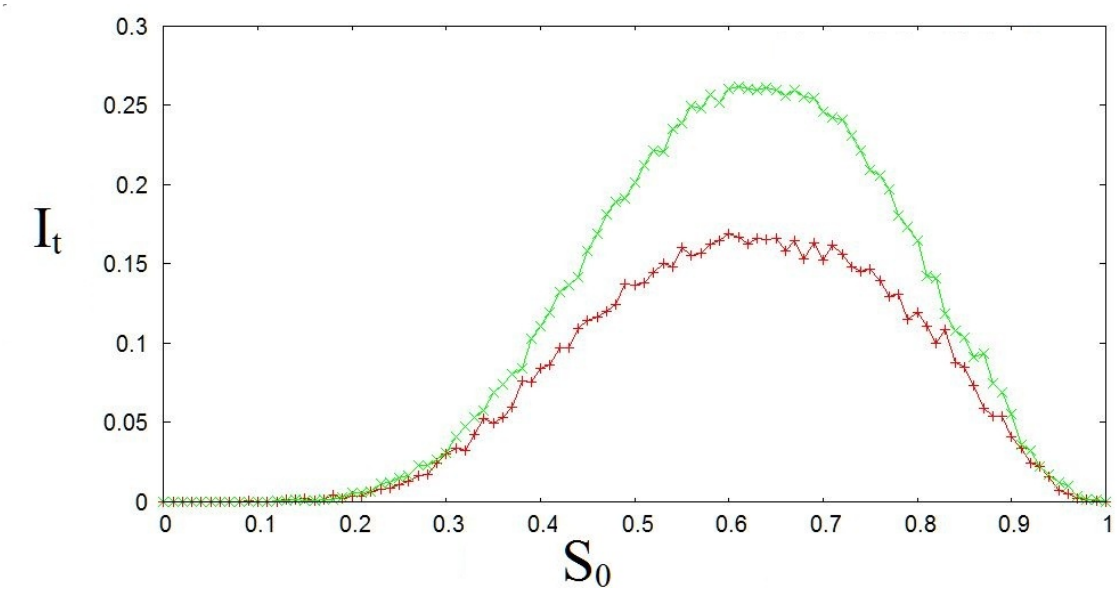

Figure 2.12: Variation of I_t (after t= 200) with S_0 (Red curve- initial infection at random site; Green curve- initial infection at the cente) [with "R" population having fixed same phase.] N= 40x40; $\tau_I = 4$; $\tau_0 = 13$, averaged over 10^3 realizations.

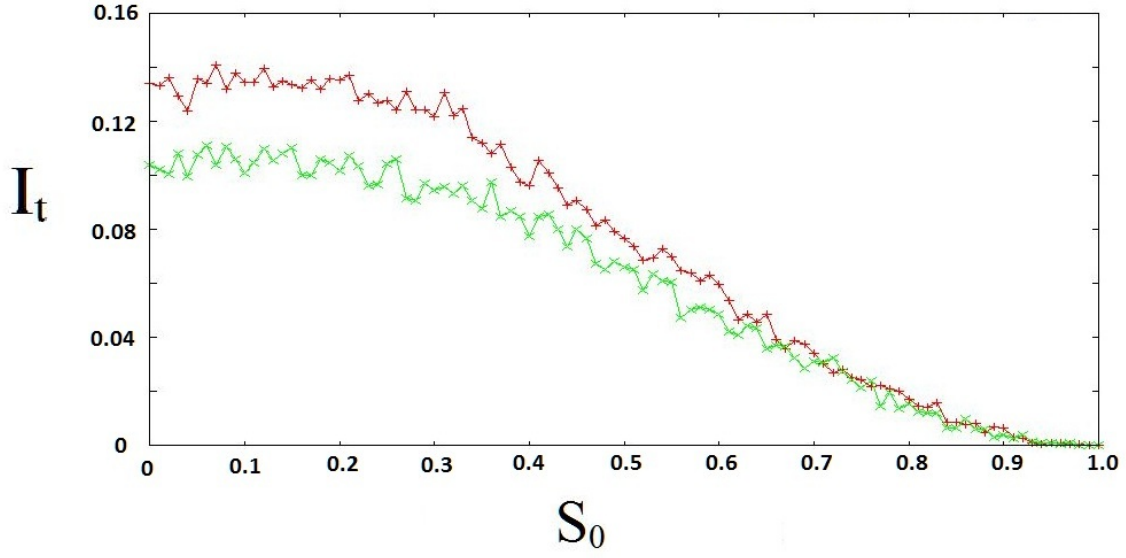

Figure 2.13: Variation of I_t (after t= 200) with S_0 (Red curve- initial infection at random site; Green curve- initial infection at the cente) [with "R" population having randomly different phases.] N= 40x40; $\tau_I = 4$; $\tau_0 = 13$, averaged over 10^3 realizations.

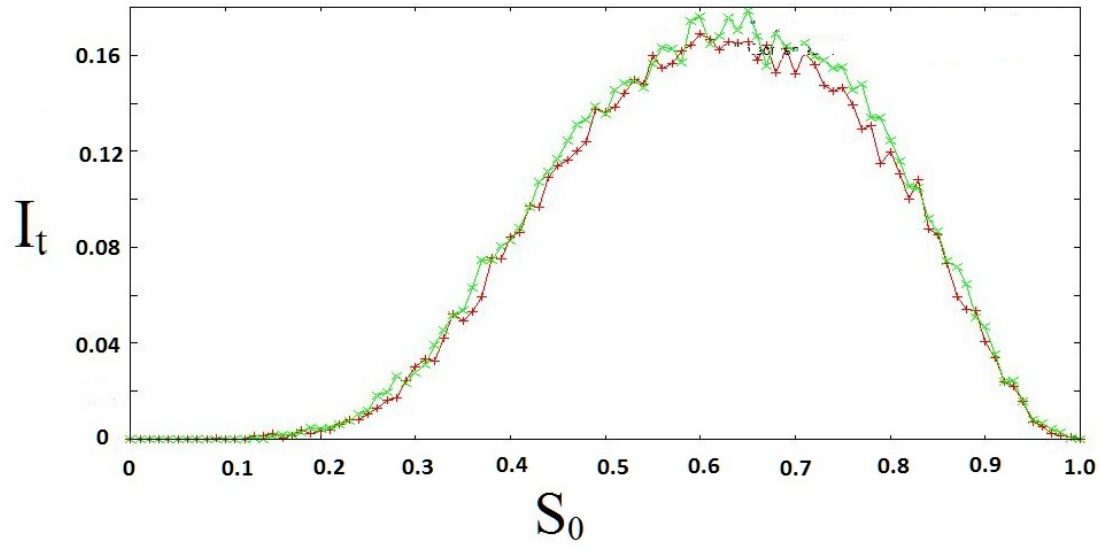

Figure 2.14: Variation of I_t (after t= 200) with S_0). N = 40x40(red curve); 100x100(green curve).[initial infection at random site]; $\tau_I = 4$; $\tau_0 = 13$, averaged over 10^3 realizations.

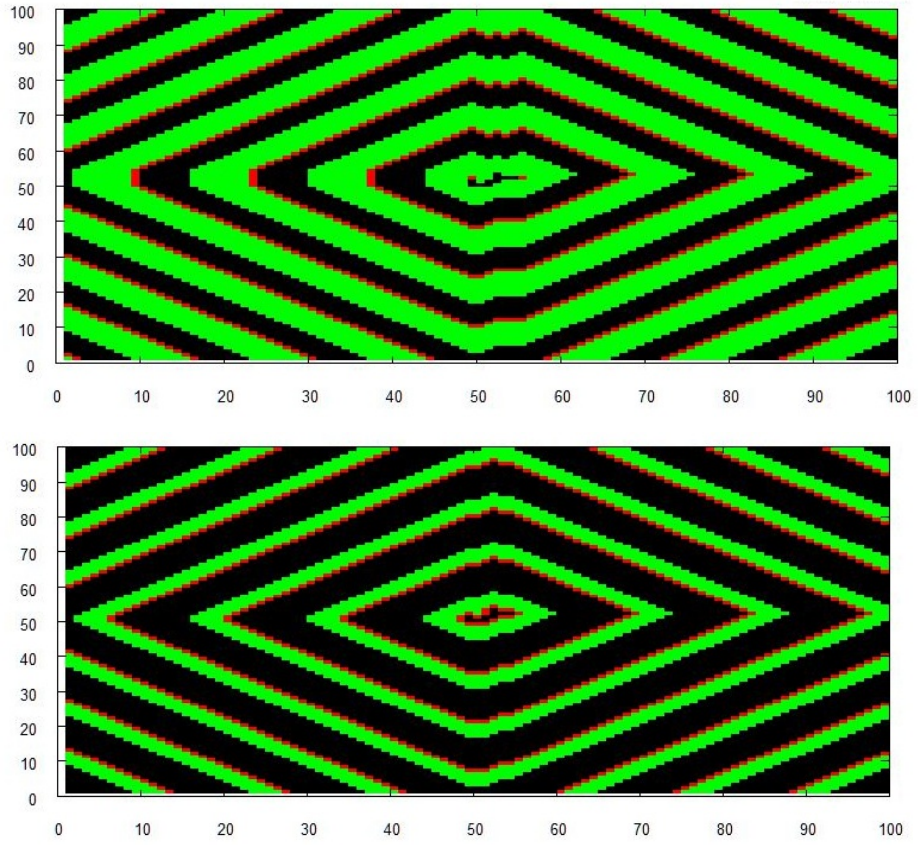

Figure 2.15: Snapshot of the infection spread pattern at t= 200 and initially infection put at the center with $\tau_I = 6$[left] & $tau_I = 9$[right]; $\tau_0 = 13$ and [S_0:$R_{fraction}$ - 0.5:0.5]. [color scheme: Green-refractory;Red-Susceptible;black-infected]

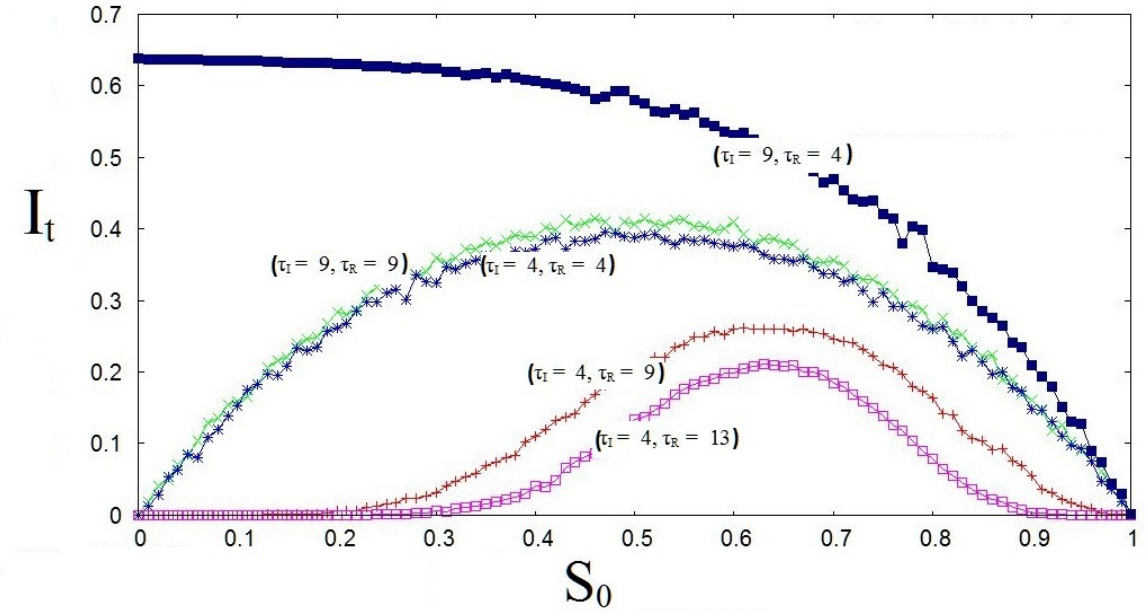

Figure 2.16: Variation of I_t (after t= 200) with S_0) for population having same phase in R $\tau_I = 4$, $\tau_R = 9$(red curve); $\tau_I = 4$, $\tau_R = 13$ (pink curve); $\tau_I = 4$, $\tau_R = 4$ (blue curve with crosses); $\tau_I = 9$, $\tau_R = 9$ (green curve); $\tau_I = 9$, $\tau_R = 4$ (blue curve with boxes). N = 40x40.[initial infection at the center]. averaged over 10^3 realizations.

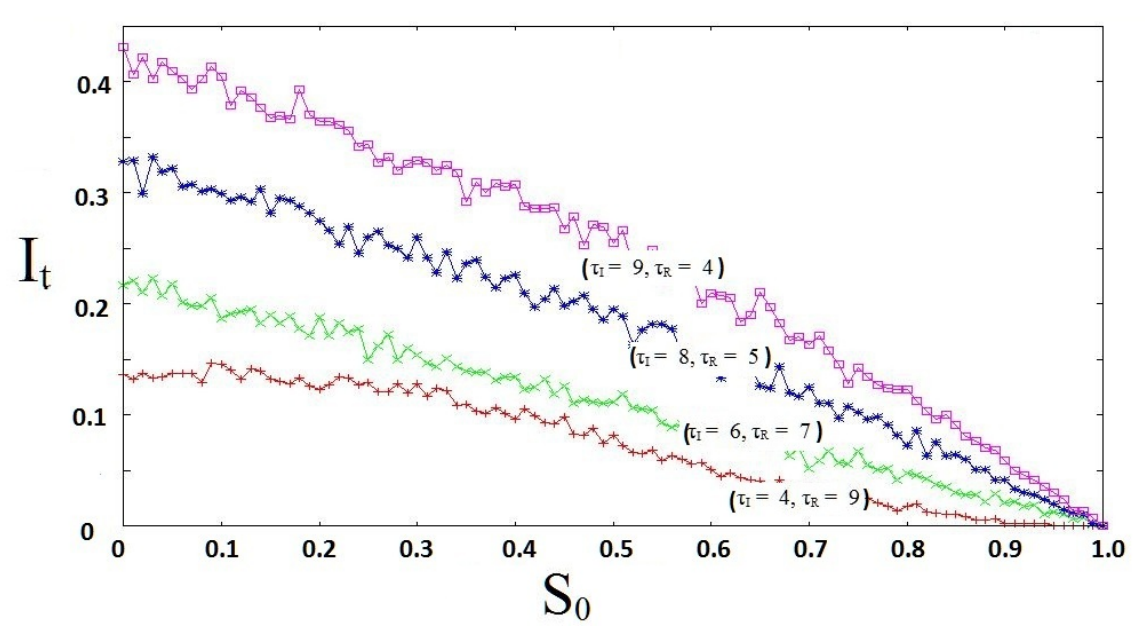

Figure 2.17: Variation of I_t (after t= 200) with S_0) for population having randomly different phase in R $\tau_I = 4$, $\tau_R = 9$(red curve); $\tau_I = 6$, $\tau_R = 7$ (green curve); $\tau_I = 8$, $\tau_R = 5$ (blue curve); $\tau_I = 9$, $\tau_R = 4$ (pink curve). N = 40x40.[initial infection at the center]. averaged over 10^3 realizations

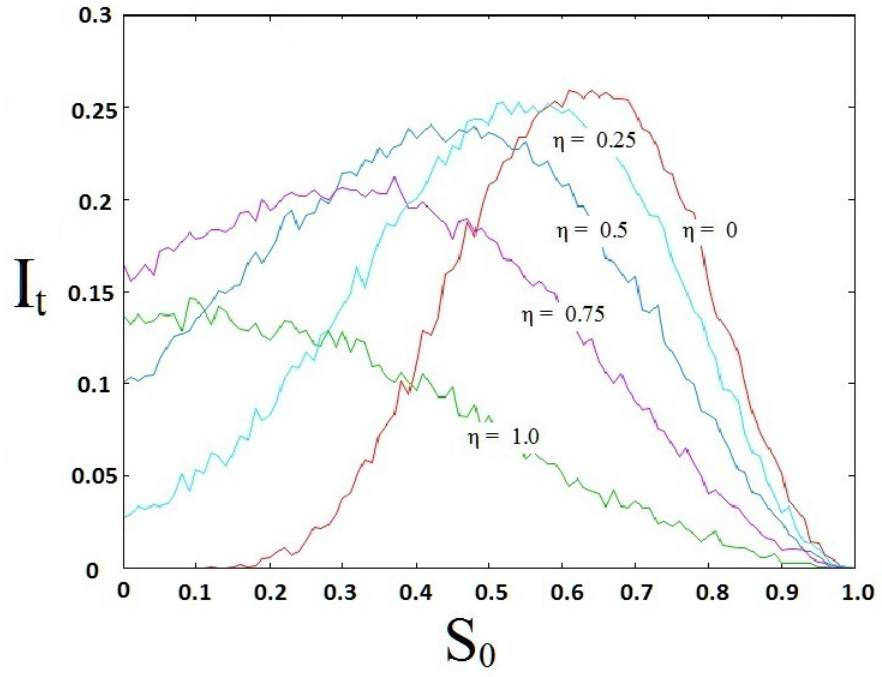

Figure 2.18: Variation of I_t (after t= 200) with S_0) (η: 0; 0.25; 0.5; 0.75; 1.0) .$\tau_I = 4$, $\tau_0 = 13$. N = 40x40.[initial infection at the center]. averaged over 10^3 realizations

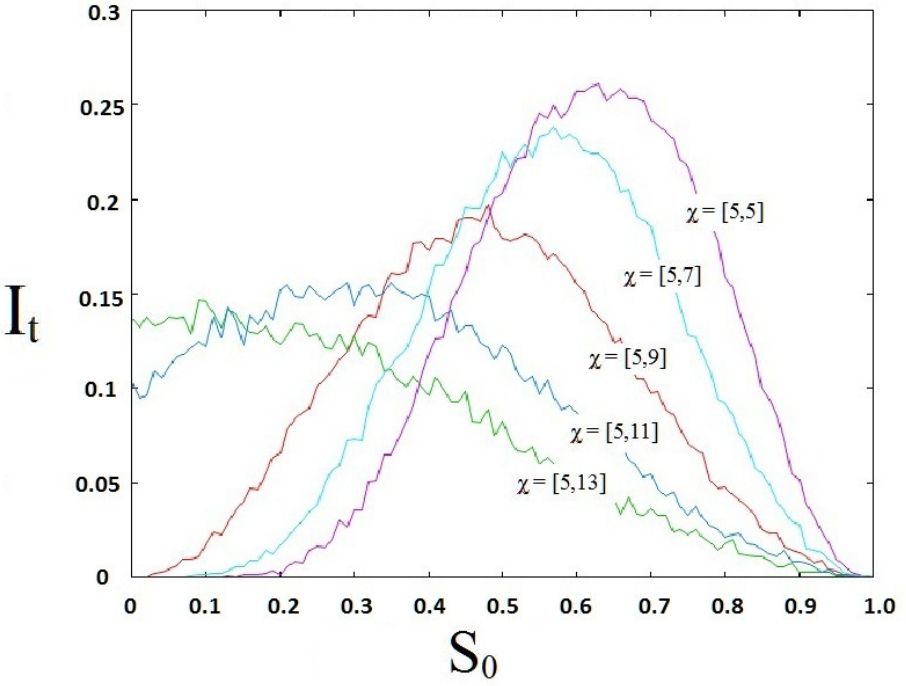

Figure 2.19: Variation of I_t (after t= 200) with S_0)(χ: [5,5]; [5,7]; [5,9]; [5,11]; [5,13]) .$\tau_I = 4$, $\tau_0 = 13$. N = 40x40.[initial infection at the center]. averaged over 10^3 realizations

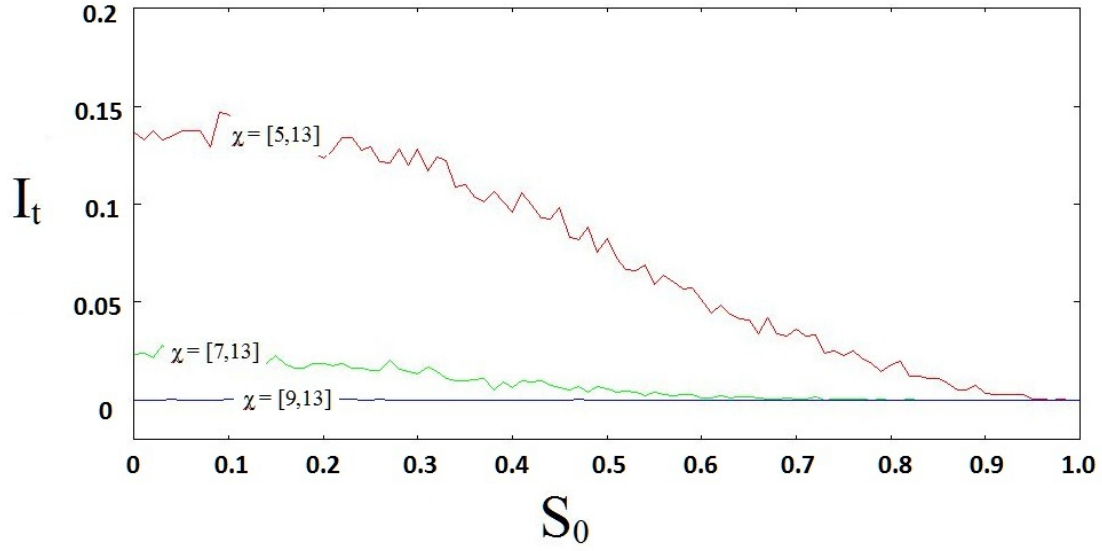

Figure 2.20: Variation of I_t (after t= 200) with S_0)(χ: [5,13]; [7,13]; [9,13]) .$\tau_I = 4$, $\tau_0 = 13$. N = 40x40.[initial infection at the center]. averaged over 10^3 realizations

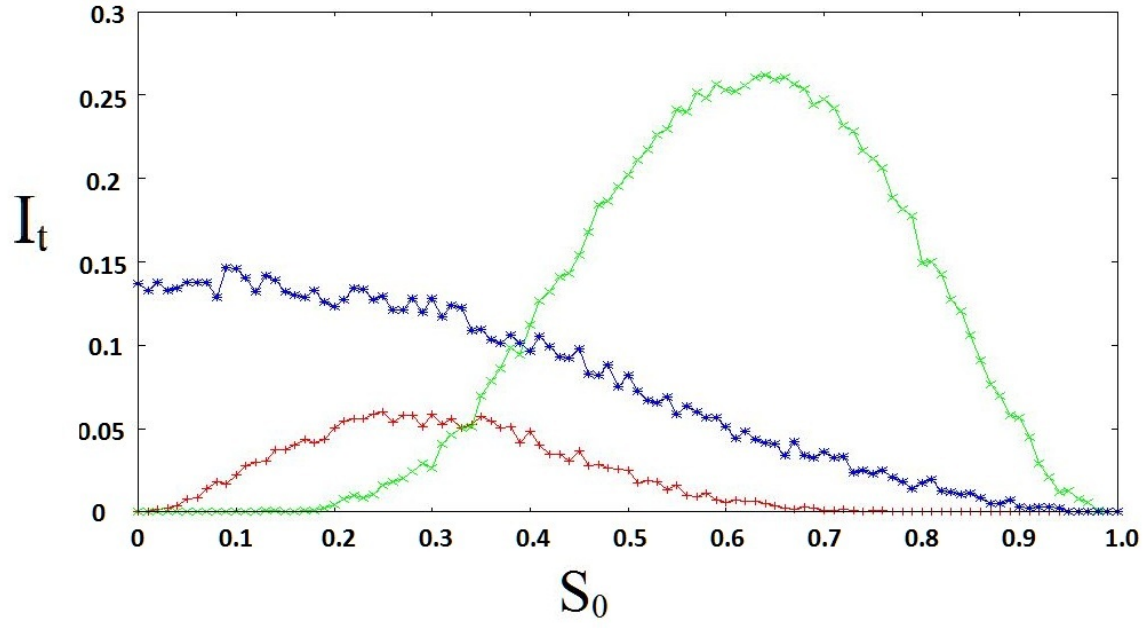

Figure 2.21: Variation of I_t (after t= 200) with S_0). Refractory population having randomly different phase in R [χ: [5,13]] (blue curve); same phase initially [$\tau_R = 9$] (red curve); same phase initially [$\tau_R = 4$] (green curve). $\tau_I = 4$, $\tau_R = 9$. N = 40x40.[initial infection at the center]. averaged over 10^3 realizations

Bibliography

[1] D J Watts and S H Strogatz, *Nature*, **393** (1998) 440–2

[2] A-L. Barabasi and R. Albert, *Science*, **286** (1999) 509–512

[3] A. Mondal, S. Sinha, and J. Kurths, *Phys. Rev. E*, **78** (2008) 066209

[4] S. Sinha, *Phys. Rev. E*, **66** (2002) 016209

[5] Varela, F., Lachaux, J.P., Rodriguez, E. & Martinerie, J., *Nat. Rev. Neurosci.* **2**, 229-239 (2001).

[6] Brezina, V., Orekhova, I.V. & Weiss, K.R., *J Neurophysiol.* **83**, 207-231 (2000).

[7] Von der Malsburg, C. *Handbook of Brain Theory and Neural Networks*,[Dynamic Link Architecture, p.365] (MIT Press, 2002).

[8] Zanette, D.H. & Gusmán, S.R., *J. Biol. Phys.* **34**, 135-148 (2008)

[9] Belykh, I. G., Belykh, V. N. & Hasler, M., *Physica D* **195**, 188-206 (2004).

[10] Amritkar, R. E., Hu, Chin-Kun, *Chaos*, **16** (2006).

[11] Kohar, V. & Sinha, S., *Chaos, Solitons & Fractals* **54**, 127-134 (2013).

[12] A. Choudhary, V. Kohar, S. Sinha, *Sci. Rep.* (Nature) **4** 2014

[13] Crutchfield, J. & Kaneko, K. in *Directions In Chaos*, [Hao, B. L.(ed.)] (World Scientific, Singapore, 1987).

[14] Barahona, M. & Pecora, L.M., *Phys. Rev. Lett.* **89**, 054101 (2002)

[15] Hong, H., Choi, M.Y. & Kim, B.J., *Phys. Rev. E* **65**, 026139 (2002)

[16] Poria, S., Shrimali, M.D. & Sinha, S., *Phys. Rev. E* **78**, 035201 (2008).

[17] Zumdieck, A., Timme, M., Geisel, T., & Wolf, F., *Phys. Rev. Lett.* **93**, 244103 (2004)

[18] 'The bubonic plague' C. McEvedy, Sci. Am. 258, No. 2, 74 (1988).

[19] 'The epidemiology of influenza' M.M. Kaplan and R.G. Webster, Sci. Am. 237, No. 6, 88 (1977).

[20] 'Island Epidemics' A. Cliff and P. Haggett, Sci. Am. 250, No. 5, 110 (1984).

[21] J.D. Murray, Mathematical Biology (Springer-Verlag, Berlin, 1993).

[22] Leah Edelstein-Keshet, Mathematical Models in Biology (Random House, New York, 1988).

[23] 'Qualitative Analyses of Communicable Disease Models' Hethcote HW. Math Bioscience, 1976; 28:335.

[24] 'Epidemiological models of Mycobacterium tuberculosis complex infections' Cagri Ozcaglar, Amina Shabbeer, Scott L. Vandenberg, Blent Yener, and Kristin P. Bennett. Math Biosci. 2012 April ; 236(2): 7796.

[25] Marcelo Kuperman, Guillermo Abramson (2001). 'Small World Effect in an Epidemiological Model.' Physical Review Letters, Vol. 86, Number 13.

[26] 'Dynamic transitions in small world networks: Approach to equilibrium limit.' Gade PM, Sinha S. Phys Rev E 2005;72:052903.

[27] Vivek Kohar, Sudeshna Sinha (2013). 'Emergence of epidemics in rapidly varying networks.' Chaos, Solitons & Fractals 54, 127-134.

[28] C.J. Rhodes, R.M. Anderson (1996). 'Dynamics in a lattice epidemic model.' Physics Letters A 210, 183-188.